

Masterthesis: Development of an improved Fitting Routine, the Classifiers Test and Reweighting of the $B \rightarrow K^* \mu \mu$ decay

Supervisors: Prof. Dr. Nicola Serra, Dr. Marcin Chzsasycz

Author: Oliver Dahme

The work presented in this thesis consists of three parts, which are all intended to be used in the contents of data analysis of data taken by the LHCb detector, especially to analyze the decay $B \rightarrow K^* \mu \mu$.

1. A new fitting routine has been developed as a more transparent and reliable alternative to the broadly used routine Minuit.
2. A test of classifiers has been performed. Classifiers are algorithms used to separate signal from background. The test in this thesis was performed to find the best classifiers in order to select events with the decay $B \rightarrow K^* \mu \mu$.
3. Third data from the Run II of the LHCb detector was used to reweight the Monte Carlo simulation of events with the decay $B \rightarrow K^* \mu \mu$.

Contents

1	Introduction	2
1.1	New fitting routine	2
1.2	Test of classifiers	3
1.3	Reweighting	3
2	RooMCMMarkovChain	3
2.1	Monte Carlo Markov Chain (MCMC)	3
2.2	Metropolis Hastings algorithm	4
2.3	Features	5
3	The LHCb Experiment	8
3.1	The LHCb Detector	9
3.2	The LHCb trigger system	11
4	The $B \rightarrow K^* \mu \mu$ decay	12
4.1	Motivation to analyze $B \rightarrow K^* \mu \mu$ decays	12
4.2	Kinematics	12
4.3	Operators for $B \rightarrow X_s l^+ l^-$ decays	14

4.4 Wilson coefficients	14
<hr/>	
5 Classifiers test	16
<hr/>	
6 Reweighting	21
6.1 Results of the $B \rightarrow K^* \mu\mu$ reweighting	22
6.2 SPlot	24
6.2.1 Likelihood method	24
6.2.2 <i>in Plot</i> technique	24
6.2.3 <i>s Plot</i> technique	25
<hr/>	
7 Outlook	27
<hr/>	
Bibliography	27
<hr/>	
A ROC curves	28
<hr/>	
B Correlation plots	39
<hr/>	
C Reweighting plots	61

1. Introduction

1.1. New fitting routine

Decay rate distributions in particle physics depend on kinematic variables as the angles between the final state particles and the energies of the particles. In order to determine the angular coefficients of the decay rate the experimentally obtained decay rates are fitted. So far this has been done with the MINUIT [2] algorithm. But as explained in detail in section 2, the MINUIT algorithm produces random errors without explanation. Furthermore MINUIT is not transparent: It is not clear, how the fit is performed, and if it really has found the global minimum.

The new algorithm implemented as part of this thesis, is called RooMCMarkovChain. It is based on a Monte Carlo Markov Chain (see section 2.1), where a certain link in the chain represents a point on the negative log-likelihood function of the fit. The chain is designed to follow the global minimum and to jump out of local minima.

RooMCMarkovChain provides two things: A fitting parameter set, for example the angular coefficients of a decay rate, at the global minimum. And one-dimensional projections of the negative log-likelihood function in the vicinity of the global minimum. They can be used for error estimations and sent along side papers which describe, how the fit has been performed. The RooMCMarkovChain will be part of the rooFit package of the ROOT Data analysis framework [1].

1.2. Test of classifiers

Raw data from a particle detector contains all kind possible decays. The first challenge of an analysis is to distinguish the one decay one wants to analyze from everything else. The common procedure to reach that goal in our days the usage of Machine Learning algorithms called Classifiers. The algorithm need two things to perform the analysis: A training dataset where signal and background is labeled accordingly, and a list of parameters that are different in signal and background. While training the algorithm will adapt thresholds on these parameters. Then, using these thresholds the algorithm is able to distinguish signal from background in unlabeled data.

The test of classifiers presented in section 5 has the goal to find the best classifier to select $B \rightarrow K^* \mu\mu$ decays in the raw data of the LHCb detector.

1.3. Reweighting

The efficiencies of all detector components have to be taken into account in data analysis. These efficiencies may be obtained by Monte Carlo simulations. Finally, Monte Carlo data and real data must match to get the correct results. Re-simulating every time everything with different parameters until the data distributions match would take too much resources. Therefore the Monte Carlo data is reweighted. Reweighting means that a weight is applied to each Monte Carlo. The weights are choosed in a way that afterwards the simulation matches the data.

2. RooMCMMarkovChain

RooMCMMarkovChain is a new class for the ROOT Data Analysis Framework [1]. You can find the install-instructions at [1]. It works best on a unix based operation system.

RooMCMMarkovChain uses a metropolis algorithm as a minimizer for the negative log likelihood function. The metropolis algorithm is based on a Monte Carlo Markov Chain and can therefore easily be scaled to multidimensional parameter space and moreover, such kind of algorithms can easily be parallelized.

2.1. Monte Carlo Markov Chain (MCMC)

A Markov Chain is a sequence of random events X_1, X_2, \dots , where the conditional distribution of X_{n+1} only depends on X_n . The space where the X_i take values is called the state space of the Markov chain, written x_1, \dots, x_n . If the conditional distribution is independent of n the Markov Chain has stationary transition probabilities. The joint distribution of a Markov chain is determined by:

- The marginal distribution of X_1 , called the initial distribution
- The conditional distribution of X_{n+1} called the transition distribution.

If the state space is finite then the initial distribution can be associated with a vector $\lambda = (\lambda_1, \dots, \lambda_n)$ defined by the following Probability Pr :

$$Pr(X_i = x_i) = \lambda_i \quad (1)$$

The transition probabilities can be associated with a matrix P having elements p_{ij} defined by:

$$Pr(X_{n+1} = x_j | X_n = x_i) = p_{ij} \quad (2)$$

That only holds if the state space is finite. Most Markov chains of interest in MCMC have an uncountable state space. The initial distribution then becomes an unconditional distribution and the transition probability distribution a conditional probability distribution.

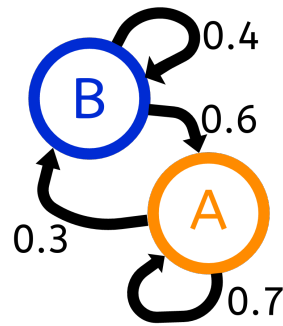


Figure 1: Illustration of states and the probability distribution to change or the stay in a state of a Monte Carlo Markov Chain. In state A there is a 0.3 probability to change into state B and a 0.7 probability to stay in state A.

2.2. Metropolis Hastings algorithm

Metropolis Hastings is a so called Monte Carlo updater. It updates the probability distribution when a change of states is proposed. That is very useful in the cases where the states are not discrete like in figure 1 but continuous. Suppose that a specified distribution has unnormalized density h . The Metropolis Hastings update does the following:

1. The current state x is proposed to move to another state with a conditional probability given x denoted as $q(x, \cdot)$.
2. The Hastings ratio to move to y is calculated:

$$r(x, y) = \frac{h(y) \cdot q(y, x)}{h(x) \cdot q(x, y)} \quad (3)$$

3. The proposed move to y is accepted with the probability $a(x, y)$:

$$a(x, y) = \min(1, r(x, y)) \quad (4)$$

This principle is used in the RooMCMMarkovChain class to minimize the negative log likelihood function. In detail a robust adaptive Metropolis hastings process is implemented. It is defined as:

1. Compute next proposed state Y_n as a random change from the current state X_{n-1} :

$$Y_n \equiv X_{n-1} + S_{n-1} U_n$$

, where U_n is an independent random vector and S_{n-1} a matrix satisfying equation 5

2. With the probability α_n the proposal is accepted and $X_n = Y_n$. Otherwise the proposal is rejected and $X_n = X_{n-1}$

$$\alpha_n \equiv \min\{1, r(X_{n-1}, Y_n)\}$$

, where r is the hastings ratio see equation 3.

3. compute the lower-diagonal matrix S_n with positive diagonal elements satisfying the equation:

$$S_n S_n^T = S_{n-1} \left(I + \eta_n (\alpha_n - \alpha^*) \frac{U_n Y_n^T}{||U_n||^2} \right) S_{n-1}^T \quad (5)$$

,where $I \in R^{d \times d}$ is the identity matrix and α^* is the forced acceptance rate.

2.3. Features

The features of the RooMCMMarkovChain class will be shown by fitting the following probability density function (pdf):

$$g(x) = \frac{1}{\sqrt{2\pi\sigma_1^2}} e^{-\frac{(x-\mu_1)^2}{2\sigma_1^2}} + f \cdot \frac{1}{\sqrt{2\pi\sigma_2^2}} e^{-\frac{(x-\mu_2)^2}{2\sigma_2^2}} \quad (6)$$

It is so called double gaus pdf, which is just the sum of two gaussian pdfs with a fractional parameter f . Where μ_1 and μ_2 are mean1 and mean2 of the two gaus and σ_1 and σ_2 the standart derviations. The result of the fit is compared with the result of the Minuit algorithm. Therfore 1000 points were simulated fowlowing the distribution 6:

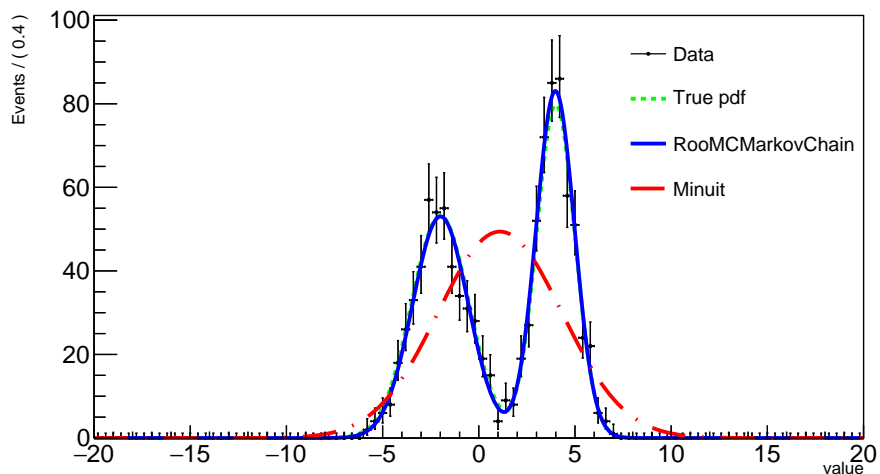


Figure 2: Fit of double gaus pdf (see equation 6) with RooMCMMarkovchain and with Minuit. The true pdf has the following values: $\mu_1 = 4$, $\sigma_1 = 1$, $\mu_2 = -2$, $\sigma_2 = 1.5$ and the fraction $f = 0.5$. The Minuit fit fails, because of a random error. The fits gets right if the starting values for the parameters are changed.

Figure 2 shows that the Minuit routine fails to fit the distribution. The reasons are unknown, but the fit gets right if the starting values of the parameters are changed. Intensive testing proved RooMCMCMarkovChain less sensitive to starting values. But one should analyze with the number of parameters usually used in particle physics, with up to 50 parameters.

The terminal output, for the fit in figure 2, gives the estimated parameters with error interval and correlation coefficients of each parameter pair.

```
RooFit v3.60 -- Developed by Wouter Verkerke and David Kirkby
Copyright (C) 2000-2013 Nikhef, University of California & Stanford University
All rights reserved, please read http://roofit.sourceforge.net/license.txt

Starting Monte Carlo Markov Chain Fit with 12000 points and cutoff after 7000 points
1% 2% 3% 4% 5% 6% 7% 8% 9% 10% 11% 12% 13% 14% 15% 16% 17% 18% 19% 20% 21% 22% 23% 24% 25% 26%
% 33% 34% 35% 36% 37% 38% 39% 40% 41% 42% 43% 44% 45% 46% 47% 48% 49% 50% 51% 52% 53% 54% 55% 5
62% 63% 64% 65% 66% 67% 68% 69% 70% 71% 72% 73% 74% 75% 76% 77% 78% 79% 80% 81% 82% 83% 84% 85
91% 92% 93% 94% 95% 96% 97% 98% 99% 100%
NO. NAME VALUE ERROR
1 frac 5.14084e-01 1.47307e-02
2 mean1 3.98243e+00 5.07205e-02
3 mean2 -1.99256e+00 7.51154e-02
4 sigma1 9.98988e-01 3.87089e-02
5 sigma2 1.44724e+00 5.86681e-02

CORRELATION COEFFICIENTS
NO. 1 2 3 4 5
1 1.000 -0.072 -0.043 0.095 -0.060
2 -0.072 1.000 0.131 -0.151 0.136
3 -0.043 0.131 1.000 -0.135 0.194
4 0.095 -0.151 -0.135 1.000 -0.171
5 -0.060 0.136 0.194 -0.171 1.000
```

Figure 3: Terminal output of the RooMCMarkovChain fit. Note that RooMCMarkovChain confused the two means, because for the algorithm the two pdfs are equal.

This gives a good initial overview of results after the fit has finished. The error calculation can be set to assume gaussian or non-gaussian errors.

In addition several other properties of the parameters can be obtained:

1. The 1 dimensional profile of the negative log likelihood function for a given parameter.

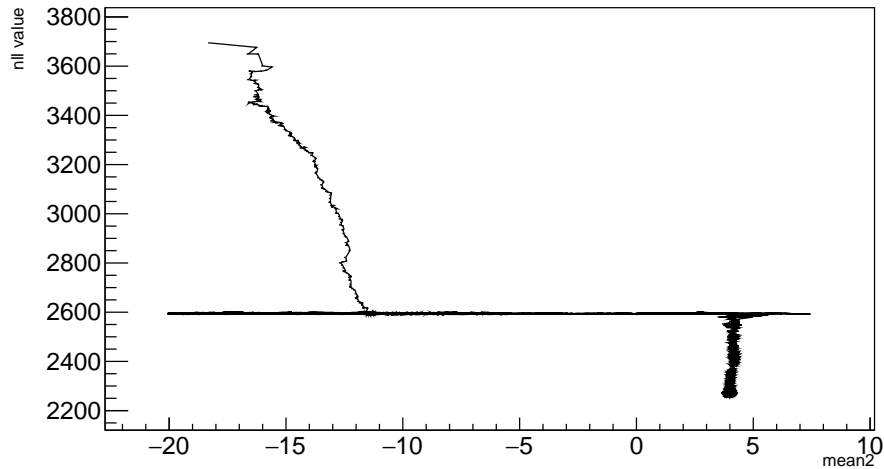


Figure 4: Profile of the negative log likelihood function for $\mu_2 = \text{mean2}$ in equation 6. There is a local minimum at the nll value of 2600, because the chain stopped going downwards.

From this plot one can see how the algorithm reached the minimum of the negative log likelihood function and if there are local minima.

2. The walk distribution of a given parameter.

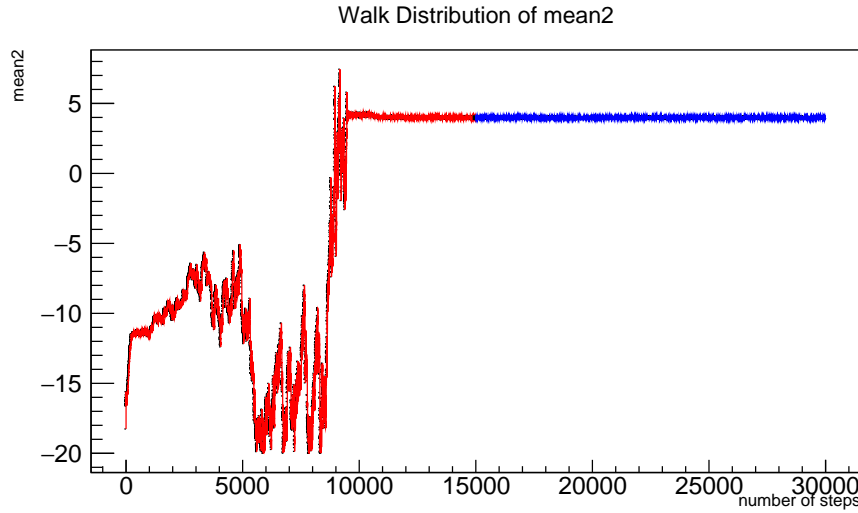


Figure 5: Walk distribution of $\mu_2 = \text{mean2}$ in equation 6. The red points are not considered for the error calculation, the number of points being cut off is defined by the user.

This plot is very important for handling the RooMCMarkovChain class. Since the error calculation is based on the variance of the walk distribution, cutting off points in the beginning greatly reduces this variance. The user has to choose how many points are cut off. Plotting the walk distribution of all parameters helps choosing the right amount. The right amount would be at the point where there is only the oscillation around the global minimum left.

3. The walk distribution of a given parameter as a histogramm.

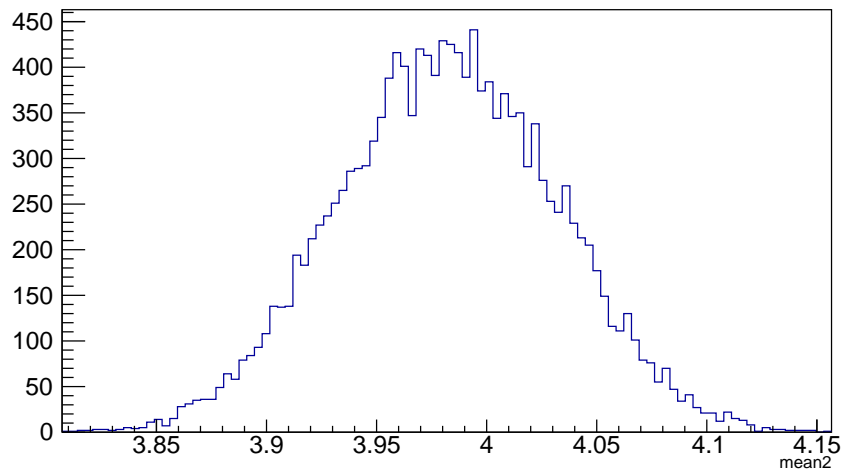


Figure 6: Walk distribution of $\mu_2 = \text{mean2}$ in equation 6 as a histogramm.

This plot can be used to check, which error strategy should be used. If the walk distribution histogramm is gaussian, gaussian errors can be assumed.

4. The scatterplot between two given parameters.

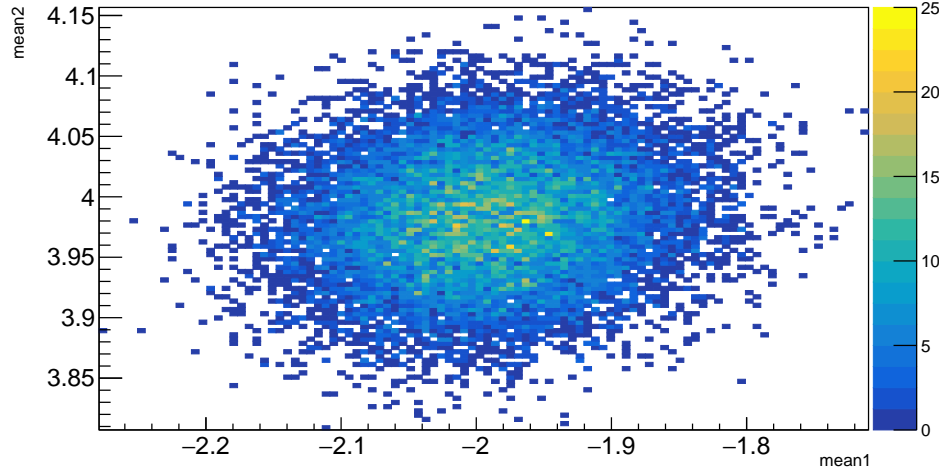


Figure 7: Scatterplot between μ_1 and μ_2 in equation 6. The round shape states that there is no correlation between the two parameters.

This plot shows the correlation between two parameters graphically.

3. The LHCb Experiment

In this section the experimental setup of the detector is presented, which recorded the data used in this thesis. The Large Hadron Collider beauty experiment (LHCb) is one of four large experiments based

at the CERN laboratory near Geneva in Switzerland. It is part of the Large Hadron Collider (LHC), a proton-proton accelerator and collider located in a vast underground tunnel with 26.7 km circumference beneath the Swiss-French countryside. The other three experiments are CMS and ATLAS which are dedicated to a wide range of physics and have therefore very large detectors. ALICE investigates quark-gluon plasma and therefore needs heavy ion collisions, instead of proton collisions.

The protons in the LHC have a kinetic energy of 7 TeV, which allows a collision energy, in the LHCb detector, of 13 TeV. In the year 2016 the LHCb had a recorded luminosity of 1906 pb^{-1} . For this thesis 2280 pb^{-1} of data, collected at LHCb during the years 2011 to 2016 are used. LHCb is dedicated to flavour physics. It therefore investigates rare decays and CP violation in beauty and charm hadrons.

CERN's Accelerator Complex

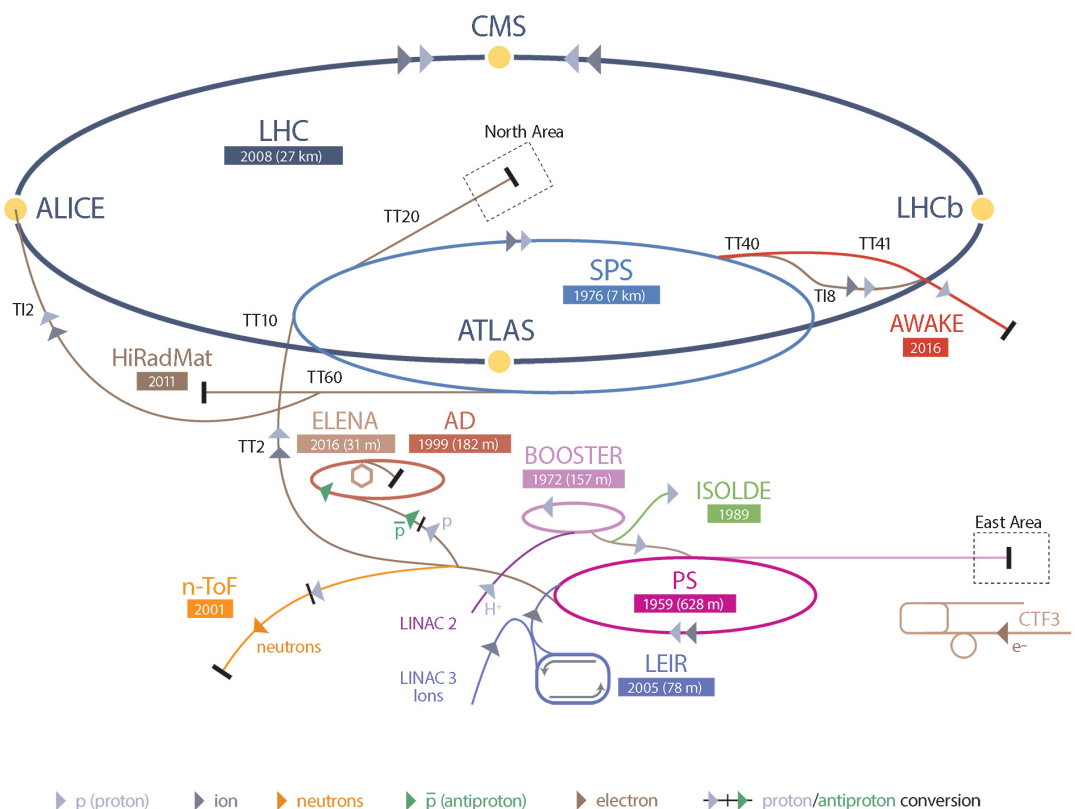


Figure 8: CERN's Accelerator Complex.[6] The protons get injected in the linear accelerator LINAC2. Then they get pre-accelerated in 3 synchrotrons (BOOSTER,PS,SPS) where the protons reach a kinetic energy of 450 GeV. That is the entering energy of the LHC which accelerates them further up to 7 TeV, before they collide at the four detectors: CMS, ATLAS, LHCb and ALICE.

3.1. The LHCb Detector

The LHCb Detector has a fixed target geometry, because beauty hadrons are mainly produced at small angles with respect to the beam pipe.

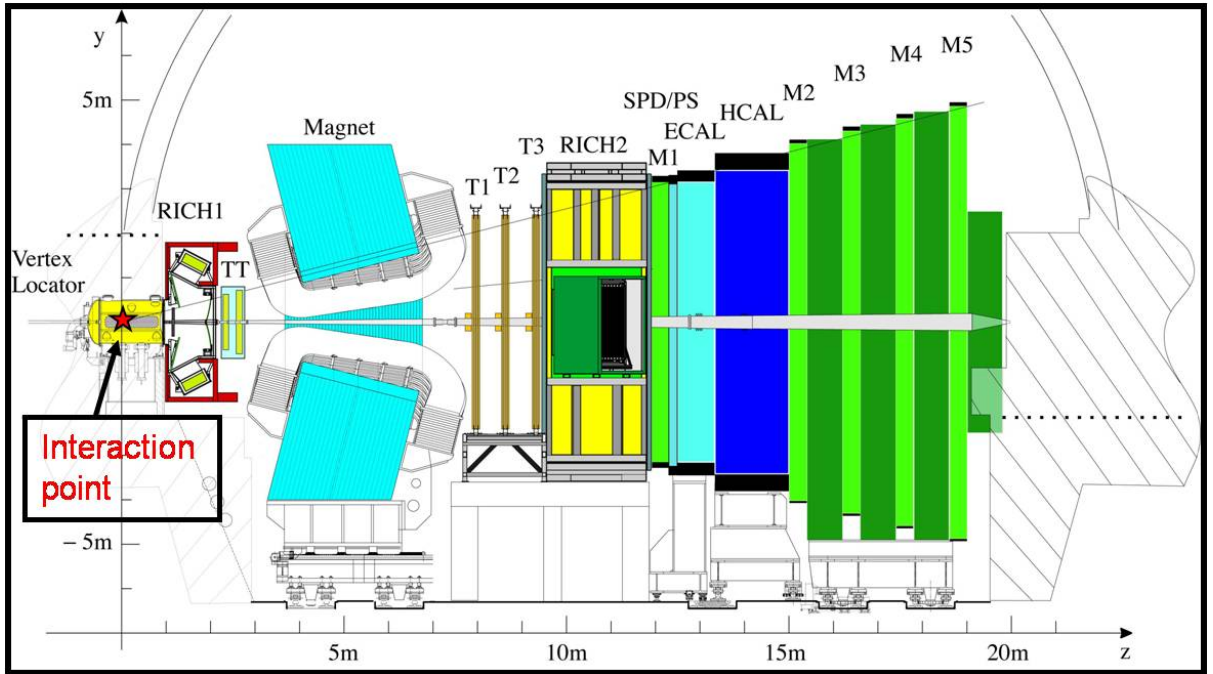


Figure 9: Basic layout of the LHCb detector [7]. The interaction point is inside the vertex detector and the beam pipe passes through the center. The different subdetectors are the two Ring Imaging Cherenkov Detectors (RICH1 and RICH2), the tracking stations (TT and T1 to T3), the scintillator pad detector (SPD), the preshower electromagnetic calorimeter (ECAL), the hadronic calorimeter (HCAL) and the muon stations (M1-M5).

VErtex LOcator (VELO) [8] : Velo picks out B mesons from the multitude of other particles produced. This is a complex task since B mesons have very short lifetimes spent close to the beam. The VELO's silicon detector elements must be placed at a distance of just five millimetres to the interaction point. To prevent damage to the detector during beam injection and stabilization it is mechanically moved to a safe distance. Velo measures B mesons indirectly by detecting its decay particles, nevertheless it has a resolution of 10 microns..

Ring Imaging Cherenkov (RICH) detectors [9] : The RICH detectors measure the emission of Cherenkov radiation, which happens when a charged particle passes through a medium faster than light does. It is a similar effect like the sonic boom a aircraft produces by breaking the sound barrier. The shape of the light cone depends on the particle's velocity, enabling the detector to determine its speed.

Magnet [10] : The big magnet of the LHCb experiment weights 27 tonnes and is mounted inside a 1,450 tonne steel frame. This powerful magnet forces all charged particles to change their trajectory. By examining the curvature of the path one can calculate its momentum.

Trackers [11] : The LHCb's tracking system consists of a series of four large rectangular stations, each covering an area of 40 m^2 . While flying through this area charged particles will leave a trace, therefore one can estimate the trajectory of a particle. The trajectory is used to link the signals left in other detector elements to the corresponding particle. In LHCb two different tracker technologies are used: The silicon tracker placed close to the beam pipe, uses silicon microstripes. If a charged particle passes such a stripe it collides with the silicon atoms, liberating electrons and creating an electric current, which is then recorded. The outer tracker situated further from the beam pipe consists of gas-filled tubes. The gas ionizes when a charged particle hits a gas molecules, producing electrons. These reach an anode wire situated in the centre of each tube. The position of the track is found by timing how long it takes

electrons to reach it.

Calorimeters [12] : Calorimeters stop particles as they pass through, measuring the amount of energy lost. In LHCb there are two different types: The electromagnetic calorimeter responsible for light particles like electrons and photons and the hadronic calorimeter responsible for heavier particles containing quarks. Both have a sandwich-like structure, with alternating layers of metal and plastic plates. If a particle hits a metal plate it produces a shower of secondary particles. These will excite polystyrene molecules in the plastic plates, which then emit ultraviolet light. The energy lost by the particle in the metal plate is proportional to the amount of UV light produced in the plastic plates.

Muon System [13] : The muon system consists of 5 rectangular stations, which cover an area of 435 m^2 . Each station has chambers filled with three gases: carbon dioxide, argon and tetrafluoromethane. Passing muons react with the mixture and electrodes detect the result.

3.2. The LHCb trigger system

The rate of events at the LHCb interaction point is 40 MHz. But the rate to have a B meson contained in the detector is 15 kHz. But the offline computing power just allows 2 kHz to be recorded. The LHCb trigger system aims to 'fill' this 2 kHz with interesting B decays and important control decays like J/ψ decays. The trigger has two levels:

The **Level Zero (L0)** trigger reduces the beginning 40 MHz to 1 MHz. To get this high rate it can only rely on fast sub-detectors as the calorimeters and the muon system. The L0 trigger looks for events with high transverse momentum with respect to the particle beam axis (p_T), because particles from a B decay have this attribute, since B Mesons are always produced almost parallel to the beam axis. In addition the L0 trigger performs a simplified vertex reconstruction with the signal of two silicon layers of the VELO to identify events with multiple proton-proton collisions. They are rejected because for this kind of events it's much more difficult to reconstruct B meson decays, since it is harder to distinguish primary and secondary vertex of the B decay.

The **High Level Trigger (HTL)** is an algorithm that runs on a farm of 1000 16-core computers. It has two stages: HLT1 which reduces the event rate to a few tens of kHz and HLT2 which reduces the rate to the 2 kHz which are recorded. HLT1 gets all the candidates of the L0 trigger and uses the full detector information on them to search for particles with a high impact parameter with respect the proton-proton collision. These particles are most likely decay products from B mesons, because of its relatively long life-time. They typically fly 1 cm away from the collision before decaying resulting in a high impact parameter for the decay products. HLT2 does a complete reconstruction of the events. It starts with the track of the VELO and connects them to the tracks in the other sub-detectors. Most important are displaced vertices, since they are strong indicator for B decays. The selection is divided into two parts. The inclusive selection searches for resonance decays like D^* or J/ψ . The exclusive selection is designed to provide the highest possible efficiency to fully reconstruct B decays of interest. It therefore uses all information available such as mass and vertex quality and intermediate resonances.

4. The $B \rightarrow K^* \mu \mu$ decay

This section describes the motivation to analyze this decay, then the operators needed to calculate the different couplings are derived and in the last section the effeteive Wilson coefficients are derived. This section is mostly theoretical and should give an overview over the decay.

4.1. Motivation to analyze $B \rightarrow K^* \mu \mu$ decays

In the Standart Model of particle physics the different leptons, Electron, Muon and Taoun only differ in there masses. Therfore if these leptons have a high energy (TeV) where the mass becomes negligible the leptons all behave the same. This phenomen is called lepton universality. For a long time it was one of the ground pillars of the Standart Model. But recent experimental results of the LHCb collaboration [3] suggest a violation of the lepton universality. They measured the branching fraction of four B deacys with a b quark to s quark transistion and two leptons in the final state. To reduce systematic uncertainties the following double ratio of these branching fractions has been considered a well defined test of lepton universaility. Since leptons at high energies should behave the same, this double ratio is expected to be equal to one.

$$R_{K^*0} = \frac{\mathcal{B}(B^0 \rightarrow K^{*0} \mu^+ \mu^-)}{\mathcal{B}(B^0 \rightarrow K^{*0} J/\psi(\rightarrow \mu^+ \mu^-))} / \frac{\mathcal{B}(B^0 \rightarrow K^{*0} e^+ e^-)}{\mathcal{B}(B^0 \rightarrow K^{*0} J/\psi(\rightarrow e^+ e^-))},$$

$$R_{K^*0} = \begin{cases} 0.66^{+0.11}_{-0.07}(\text{stat}) \pm 0.03(\text{syst}) & \text{for } 0.045 < q^2 < 1.1 \text{GeV}^2/c^4, \\ 0.69^{+0.11}_{-0.07}(\text{stat}) \pm 0.05(\text{syst}) & \text{for } 1.1 < q^2 < 6.0 \text{GeV}^2/c^4. \end{cases} \quad (7)$$

The mesurement shows a 2.1-2.3 and 2.4-2.5 σ deviation from the Standart Modell in the two q^2 regions, respectively. To investigate further the same measurment is performed with new data from the LHCb detector. The goal of this thesis is to contribute to this new measuremnt.

4.2. Kinematics

In this section the decay itself and its kinematics are explained: The Decay is a flavor changing neutral current (FCNC) with four charged particles in the final state. The FCNC is a current, which changes the falvor of a fermion without changing its electric charge. The four particles in the final stage are: The K^+ and π^- from the K^* decay and two leptons from the loop or box diagrams:

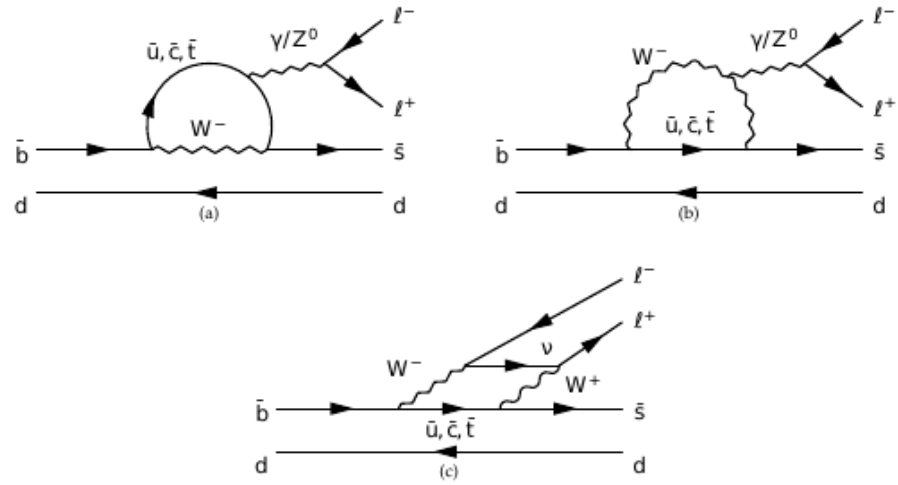


Figure 10: Feynman diagrams for decay $B(\bar{b},d) \rightarrow K^*(\bar{s},d) l^+ l^-$ at lowest order

The kinematics of the decay are defined by the three angles θ_K , θ_L and ϕ , shown in figure 11 and the invariant di-muon mass square q^2 .

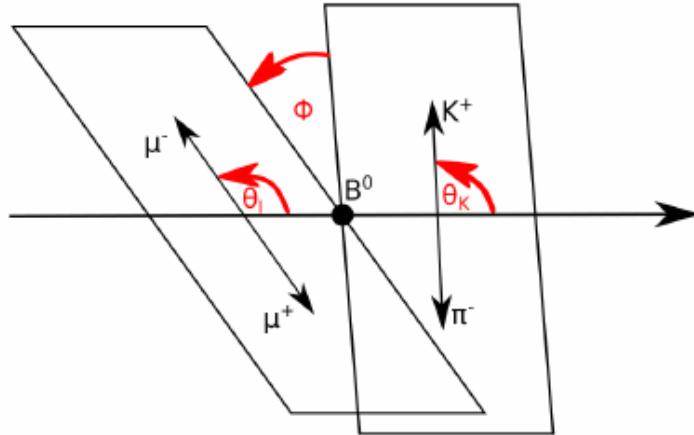


Figure 11: kinematic variables of the decay $B^0 \rightarrow K^{*0} \mu^+ \mu^-$

The differential decay rate for the B^0 Meson can be expressed in terms of these variables:

$$\frac{d^4\Gamma}{d \cos \theta_L d \cos \theta_K d \phi d q^2} = \frac{9}{32\pi} I(q^2, \theta_L, \theta_K, \phi)$$

with: $I(q^2, \theta_L, \theta_K, \phi) = I_1^S \sin^2(\theta_K) + I_1^C \cos^2 \theta_K + (I_2^S \sin^2 \theta_K + I_2^C \cos^2 \theta_K) \cos^2 \theta_L$

$$+ I_3 \sin^2 \theta_K \sin^2 \theta_L \cos 2\phi + I_4 \sin 2\theta_K \sin 2\theta_L \cos \phi \quad (8)$$

$$+ I_5 \sin 2\theta_K \sin \theta_L \cos \phi$$

$$+ (I_6^S \sin^2 \theta_K + I_6^C \cos^2 \theta_K) \cos \theta_L + I_7 \sin 2\theta_K \sin \theta_L \sin \phi$$

$$+ I_8 \sin 2\theta_K \sin 2\theta_L \sin \phi + I_9 \sin^2 \theta_K \sin^2 \theta_L \sin 2\phi$$

This decay rate is defined as the probability per unit time that the particle will decay. The I_i can be obtained by fitting this decay rate to the kinematic variables obtained by the detector. This fit is usually done by a standard fitting routine called MINUIT [2]. In section 2 an alternative is presented.

For completeness the next two sections describe some of the theory concerning the decay: The operators and wilson coefficients.

4.3. Operators for $B \rightarrow X_s l^+ l^-$ decays

In this section all the operators of the decay are derived from the effective Lagrangian. the operators in Quantum field theory are used to create or destroy particles, by applying them to a quantum field. This section should just give an overview if you need more detailed information consider reading [4].

The effective Lagrangian for $B \rightarrow X_s l^+ l^-$ decays has the form:

$$\begin{aligned} \mathcal{L}_{eff} = & \mathcal{L}_{QCD,QED}(u, d, s, c, b, e, \mu, \tau) \\ & + \frac{4G_F}{\sqrt{2}} [V_{us}^* V_{ub} (C_1^c P_1^u + C_2^c P_2^u) + V_{cs}^* V_{cb} (C_1^c P_1^c + C_2^c P_2^c)] \\ & + \frac{4G_F}{\sqrt{2}} \sum_{i=3}^{10} [(V_{us}^* V_{ub} + V_{cs}^* V_{cb}) C_i^c + V_{ts}^* V_{tb} C_i^t] P_i. \end{aligned} \quad (9)$$

The first term in equation 9 contains the kinetic terms of the light SM particles as well as their QCD and QED interactions. The remaining two terms consist of $\Delta B = -\Delta S = 1$ local operators of dimension ($d \leq 6$), which contain those light fields. The mass of the s quark can be neglected in comparison with the b mass. One gets the following operators:

$$\begin{aligned} \mathcal{O}_1^u &= (\bar{s}_L \gamma_\mu T^a u_L)(\bar{u}_L \gamma^\mu T^a b_L), & \mathcal{O}_6 &= (\bar{s}_L \gamma_{\mu_1} \gamma_{\mu_2} \gamma_{\mu_3} T^a b_L) \sum_q (\bar{q} \gamma^{\mu_1} \gamma^{\mu_2} \gamma^{\mu_3} T^a q), \\ \mathcal{O}_2^u &= (\bar{s}_L \gamma_\mu u_L)(\bar{u}_L \gamma^\mu b_L), & \mathcal{O}_7 &= \frac{e}{g^2} m_b (\bar{s}_L \sigma^{\mu\nu} b_R) F_{\mu\nu}, g \\ \mathcal{O}_1^c &= (\bar{s}_L \gamma_\mu T^a c_L)(\bar{c}_L \gamma^\mu T^a b_L), g & \mathcal{O}_8 &= \frac{1}{g} m_b (\bar{s}_L \sigma^{\mu\nu} T^a b_R) G_{\mu\nu}^a, \\ \mathcal{O}_2^c &= (\bar{s}_L \gamma_\mu c_L)(\bar{c}_L \gamma^\mu b_L), & \mathcal{O}_9 &= \frac{e^2}{g^2} (\bar{s}_L \gamma_\mu b_L) \sum_l (\bar{l} \gamma^\mu l), \\ \mathcal{O}_3 &= (\bar{s}_L \gamma_\mu b_L) \sum_q (\bar{q} \gamma^\mu q), & \mathcal{O}_{10} &= \frac{e^2}{g^2} (\bar{s}_L \gamma_\mu b_L) \sum_l (\bar{l} \gamma^\mu \gamma_5 l), \\ \mathcal{O}_4 &= (\bar{s}_L \gamma_\mu T^a b_L) \sum_q (\bar{q} \gamma^\mu T^a q), & & \end{aligned} \quad (10)$$

where \sum_q and \sum_l denote the sums over light quarks and all leptons, respectively.

4.4. Wilson coefficients

In this section the Wilson coefficients are derived from the effective Hamiltonian of the decay. The effective Hamiltonian for $b \rightarrow s \mu^+ \mu^-$ transitions can be written as:

$$H_{eff} = -\frac{4G_F}{\sqrt{2}} \left(\lambda_t H_{eff}^{(t)} + \lambda_u H_{eff}^{(u)} \right) \quad (11)$$

The λ_i can be expressed with CKM combinations $\lambda_i = V_{ib} V_{is}^*$.

$$H_{eff}^{(t)} = C_1 \mathcal{O}_1^c + C_2 \mathcal{O}_2^c + \sum_{i=3}^6 C_i \mathcal{O}_i + \sum_{i=7,8,9,10,P,S} (C_i \mathcal{O}_i + C'_i \mathcal{O}'_i) \quad (12)$$

$$H_{eff}^{(u)} = C_1 (\mathcal{O}_1^c - \mathcal{O}_1^u) + C_2 (\mathcal{O}_2^c - \mathcal{O}_2^u). \quad (13)$$

The contribution of $H_{eff}^{(u)}$ has a double Cabibbo suppression and is therefore usually dropped. It is kept here since it is sensitive to complex phases of decay amplitudes. The operators $P_{i \leq 6}$ are the same as for general $B \rightarrow X_s l^+ l^-$ decays, see equation 10. The remaining ones are given by:

$$\begin{aligned} \mathcal{O}_7 &= \frac{e}{g^2} m_b (\bar{s} \sigma_{\mu\nu} P_R b) F^{\mu\nu}, & \mathcal{O}'_7 &= \frac{e}{g^2} m_b (\bar{s} \sigma_{\mu\nu} P_L b) F^{\mu\nu}, \\ \mathcal{O}_8 &= \frac{1}{g} m_b (\bar{s} \sigma_{\mu\nu} T^a P_R b) G^{\mu\nu a}, & \mathcal{O}'_8 &= \frac{1}{g} m_b (\bar{s} \sigma_{\mu\nu} T^a P_L b) G^{\mu\nu a}, \\ \mathcal{O}_9 &= \frac{e^2}{g^2} (\bar{s} \sigma_\mu P_L b) (\bar{\mu} \gamma^\mu \mu), & \mathcal{O}'_9 &= \frac{e^2}{g^2} (\bar{s} \gamma_\mu P_R b) (\bar{\mu} \gamma^\mu \mu), \\ \mathcal{O}_{10} &= \frac{e^2}{g^2} (\bar{s} \gamma_m u P_L b) (\bar{\mu} \gamma^\mu \gamma_5 \mu), & \mathcal{O}'_{10} &= \frac{e^2}{g^2} (\bar{s} \gamma_\mu P_R b) (\bar{\mu} \gamma^\mu \gamma_5 \mu), \\ \mathcal{O}_S &= \frac{e^2}{16\pi^2} m_b (\bar{s} P_R b) (\bar{\mu} \mu), & \mathcal{O}'_S &= \frac{e^2}{16\pi^2} m_b (\bar{s} P_L b) (\bar{\mu} \mu), \\ \mathcal{O}_P &= \frac{e^2}{16\pi^2} m_b (\bar{s} P_R b) (\bar{\mu} \gamma_5 \mu), & \mathcal{O}'_P &= \frac{e^2}{16\pi^2} m_b (\bar{s} P_L b) (\bar{\mu} \gamma_5 \mu), \end{aligned} \quad (14)$$

where m_b denotes the running b mass in the \overline{MS} scheme and g is the strong coupling constant and $P_{L,R} = (1 \pm \gamma_5)/2$. In the Standart Modell the primed Operators with opposite chirality to the unprimed operators vanish or are highly suppressed as are the \mathcal{O}_S and \mathcal{O}_P . The contributions of $\mathcal{O}_{1,2,3,4,5,6}$ are neglected, since they are either heavily constrained or their impact turns out to be generically very small. For example in the left-right symmetric models or throughout gluino contributions in a general Minimal Supersymmetric Standard Model.

The C_i coefficients in the equations 12 and 13 are called Wilson coefficients. They encode short-distance physics and New Physics effects. For the calculation a matching scale $\mu = m_W$ is chosen, in a perturbative expansion in powers of $\alpha_s(m_W)$. Then the Wilson coefficients are evolved down to scales $\mu = m_b$ according to the solutions of the renormalization group equations. Contributions by New Physics enter through $C_i(m_W)$, while the low scales are determined by the Standart Modell. To allow a more organized expansion of the Wilson coefficients in perturbation theory the factors $16\pi^2/g^2 = 4\pi/\alpha_S$ are included into the definitions of the operators $\mathcal{O}_{i \geq 7}$. All the C_i expand as:

$$C_i = C_i^{(0)} + \frac{\alpha_s}{4\pi} C_i^{(1)} + \left(\frac{\alpha_s}{4\pi}\right)^2 C_i^{(2)} + O(\alpha_s^3) \quad (15)$$

where $C_i^{(0)}$ is the tree-level contribution, which is equal to zero for all operators except \mathcal{O}_2 and $C_i^{(n)}$ denotes the n-loop contributions. Before discussing the Wilson coefficients in details, lets look at the Operators again; the operators \mathcal{O}'_S and \mathcal{O}'_P are given in terms of conserved currents. They carry no scale-dependence. They do not mix with other operators and their Wilson coefficients are at the matching scale. \mathcal{O}_9 is also given by conserved currents. It mixes with $\mathcal{O}_{1,2,3,4,5,6}$ via a virtual photon decaying into $\mu^+ \mu^-$. In addition there is a scale dependence from the factor $1/g^2$. This dependence is also present in \mathcal{O}_{10} which otherwise would be scale independent.

C_7 and C_9 always appear in a particular combination with other Wilson coefficients in matrix elements.

Therefore effective coefficients are defined:

$$\begin{aligned} C_7^{eff} &= \frac{4\pi}{\alpha_s} C_7 - \frac{1}{3} C_3 - \frac{4}{9} C_4 - \frac{20}{3} C_5 - \frac{80}{9} C_6, \\ C_8^{eff} &= \frac{4\pi}{\alpha_s} C_8 + C_3 - \frac{1}{6} + 20C_5 - \frac{10}{3} C_6, \\ C_9^{eff} &= \frac{4\pi}{\alpha_s} C_9 + \mathcal{Y}(q^2), \\ C_{10}^{eff} &= \frac{4\pi}{\alpha_s} C_{10}, \\ C_{7,8,9,10}'^{eff} &= \frac{4\pi}{\alpha_s} C'_{7,8,9,10}, \end{aligned} \quad (16)$$

$$\begin{aligned} \text{where } \mathcal{Y}(q^2) &= h(q^2, m_c) \left(\frac{4}{3} C_1 + C_2 + 6C_3 + 60C_5 \right) \\ &\quad - \frac{1}{2} h(q^2, m_b) \left(7C_3 + \frac{4}{3} C_4 + 76C_5 + \frac{64}{3} C_6 \right)_{env} \\ &\quad - \frac{1}{2} h(q^2, 0) \left(C_3 + \frac{4}{3} C_4 + 16C_5 + \frac{64}{3} C_6 \right) \\ &\quad + \frac{4}{3} C_3 + \frac{64}{9} C_5 + \frac{64}{27} C_6. \end{aligned} \quad (17)$$

The function $h(q^2, m_q)$ comes from the fermion loop and for completeness is presented in equation 18 below. If you need more details consider reading [5].

$$\begin{aligned} h(q^2, m_q) &= -\frac{4}{9} \left(\ln \frac{m_q^2}{\mu^2} - \frac{2}{3} - z \right) - \frac{4}{9} (2+z) \sqrt{|z-1|} \cdot \begin{cases} \arctan \frac{1}{\sqrt{z-1}} & z > 1 \\ \ln \frac{1+\sqrt{1-z}}{\sqrt{z}} - \frac{i\pi}{2} & z \leq 1 \end{cases} \\ z &= \frac{4m_q^2}{q^2} \end{aligned} \quad (18)$$

5. Classifiers test

In particle physics the first step of each analysis is to clean up the data. That means to subtract the background from the signal. Signal means for example a type of decay like the $B \rightarrow K^*\mu\mu$ decay. To find this decay in the raw data of a detector which contains all kind of decays one needs thresholds on experimental parameters which are different or in the best case unique to the decay. That can be all kind of parameters like vertex locations, momentas or angles between trajectories. For the $B \rightarrow K^*\mu\mu$ decay these parameters would be:

- Decay vertex location for reconstructed particles (ENDVERTEX)
- Primary vertex location (OWNPV)
- Impact parameter (IP_OWNPV)
- Flight distance (FD_OWNPV)
- The cosine of the angle between primary vertex and decay vertex and recorded momentum (DIRA_OWNPV)

The names in the braces are the labels given to these parameters in the data structure of the ROOT Data Analysis Framework [1]. Now one needs thresholds on these parameters, which define the signal-region. For example the flight distance has to be between 0.2 milimeters and 2 centimeters. But how do you obtain these thresholds? Thats were Classifiers are usefull. Classifiers are a type of algorithm

from the Machine Learning area. They can be trained to distinguish different types of data. In this case signal and background. Each event in the data gets a probability to be signal assigned to it. So after the classification one can just take all the events with a probability over lets say 80%. One has now eliminated 80% of the background and can continue cleaning up the signal but that's not a part of this thesis. The goal of this part was to find the best classifier to be used in the $B \rightarrow K^* \mu \mu$ decay analysis.

Seven different classifiers were tested. A test means that the classifier is given a training set consisting of Monte Carlo simulated events containing only $B \rightarrow K^* \mu \mu$ decays and randomly chosen real detector data, containing all kinds of decays. In a training set the data is labeled. The Monte Carlo events are labeled with 1 for signal and the real data with 0 for background. The classifier will now train, that means the algorithm tries to label the data into signal and background by choosing different thresholds on the parameters mentioned above. After the training the thresholds get fixed. Now one has to test the classifier to check if everything worked fine. To do so a second set of data is prepared similar to the training set, just that the labels are now hidden from the classifier. Since the classifiers are not perfect, they do not assign 0 and 1 to each event but rather a probability to be signal between 0 and 1. A good classifier will now label the signal events with a high probability and background with a low probability. A bad classifier will assign 0.5 probability to each event. With a 0.5 probability no information was gained by classification, because having a 50:50 chance is as good as guessing. This probability assignments can now be used as a threshold themselves.

Another property of classifiers is, that the data used in the training, can no longer be used in the analysis, because the classifier knows the training set too well and a bias is introduced if one reuses the training data in the actual analysis. That would mean that the part of the real detector data which is needed to train the classifiers would be lost for further analysis. To avoid such a waste of data a technique called k-folding is used.

K-folding means that no training set is created. But the data Monte Carlo Mix with signal events and all kinds of other events is split into k equal parts. Now to classify one part all the other parts are used for training. After iterating over all parts, one has classified all the data without losing any. The only disadvantage are the additional computer resources needed, since the classifier has now to be trained k times instead of one time.

The following list of classifiers were tested and compared in terms of performance:

- Ada Boost [14]
- uGB [15] + knnAda (k-nearest neighbor AdaBoost)
- uBoost [16]
- uGB [15] + Fl (flatness loss)
- xgb [17]
- sk_bdtg [18]
- sk_bdt [19]

The test was performed with 30000 events from the 2016 LHCb $B \rightarrow K^* \mu \mu$ data and 10000 events from the Monte Carlo simulation.

To compare classifiers the so called ROC (receiver operating characteristic) curves are used. The ROC curve shows the true positive rate against the false positive rate. The true positive rate is the rate of signal events that have been classified correctly as signal events, while the false positive rate is the rate of background events classified as signal events. On figure 12 a ROC curves of the classifiers above is displayed. The sample of 40000 events to test the classifiers was cut into ten equal parts, also called

folds. In figure 12 the ROC curve of one of these folds is displayed, the other nine can be found in the appendix A.

It turns out that all the classifiers classify the data mostly correctly with just some minor variances. The ROC curve is in that case not a good tool to compare the different classifiers.

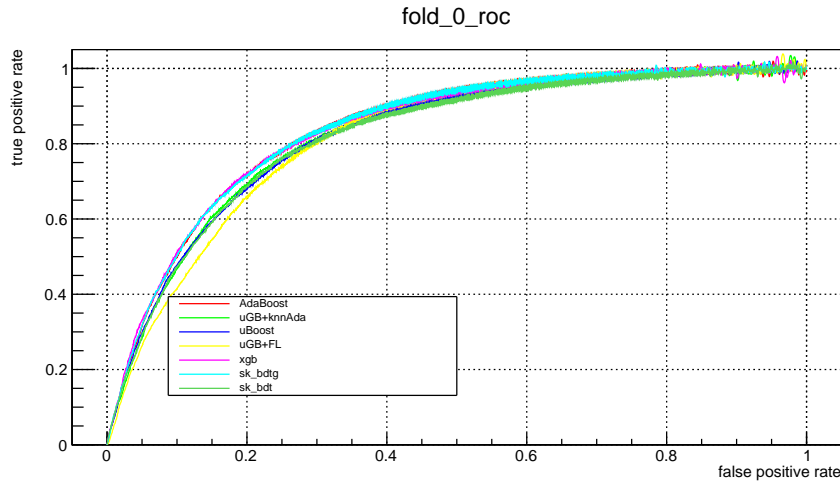


Figure 12: ROC curve of the first fold. One can see that all the classifiers are competitive in terms of classifying correctly

The next step is to check for correlations between the assigned probabilities and the kinematic variables. The kinematic variables as explained in section 4.2 are used to obtain the angular coefficients of the decay rate. If there is a correlation between the assigned probabilities from the classifier and these variables, a peak is artificially added into the distribution of these variables. Imagine a positive correlation between the B mass in the range 5000 to 6000 GeV and the probability to be signal. After cutting at lets say 0.8 probability there will be a peak in the B mass distribution between 5000 and 6000 GeV. Normally such a peak suggest a new particle in this range. This is to avoid at all cost since it will compromise the whole analysis later on.

In the following the correlation between the probability to be signal assigned by the classifier and the B mass are shown. The correlation plots for the other kinematic variables can be found in appendix B.

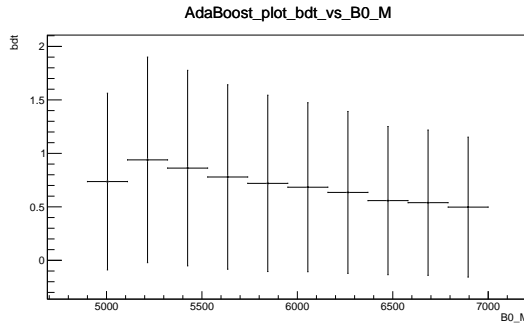


Figure 13: This plot shows the probabilities assigned by the classifier as explained in the above paragraph, labeled with bdt on the Y axis. On the X axis the values for the B mass are shown. The X - errorbars indicate the length of each bin, while the Y errorbars represent the standard deviation on the probabilities. One can see in this plot the correlation between the classifiers probabilities and the B mass for the AdaBoost classifier. There is a obvious correlation from the second bin to the fourth bin.

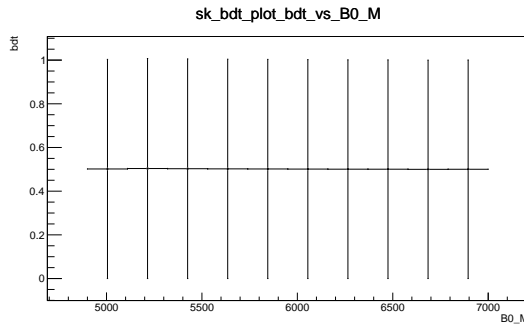


Figure 14: This plot shows the correlations between the probabilities to be signal assigned by the sk_bdt classifier and the B mass. There is no correlation.

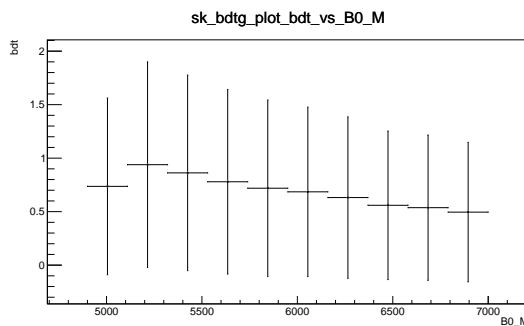


Figure 15: This plot shows the correlations between the probabilities to be signal assigned by the sk_bdtg classifier and the B mass. There is a obvious correlation from the second bin to the fourth bin.

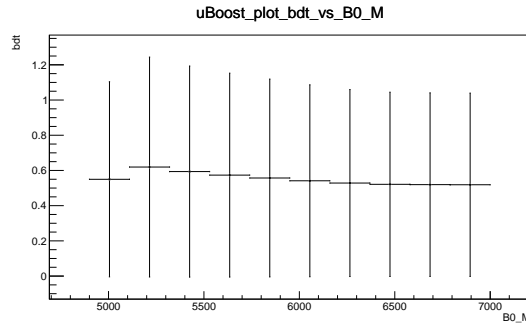


Figure 16: This plot shows the correlations between the probabilities to be signal assigned by the uBoost classifier and the B mass. There is just a very small correlation compared to other classifiers.

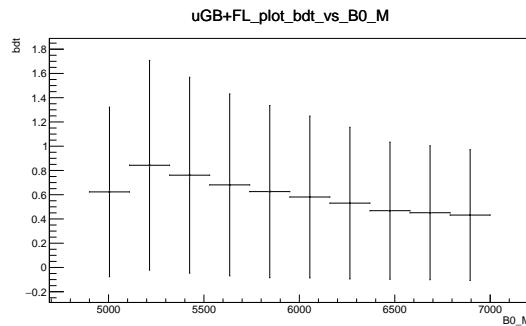


Figure 17: This plot shows the correlations between the probabilities to be signal assigned by the uGB+FL classifier and the B mass. There is a obvious correlation from the second bin to the fourth bin.

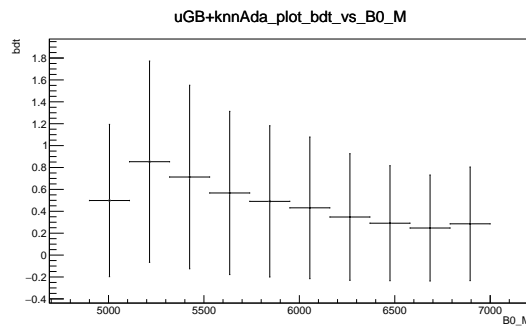


Figure 18: This plot shows the correlations between the probabilities to be signal assigned by the ugb+knnAda classifier and the B mass. There is a obvious correlation from the second bin to the fourth bin.

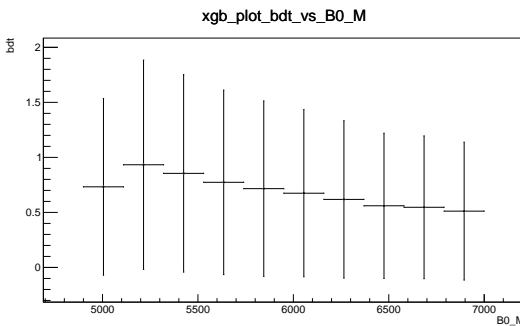


Figure 19: This plot shows the correlations between the probabilities to be signal assigned by the xgb classifier and the B mass. There is a obvious correlation from the second bin to the fourth bin.

The two classifiers with the least correlation are the sk_bdt and the uBoost classifiers. Therfore they could be used to do seperate between signal and background in the $B \rightarrow K^* \mu\mu$ data.

6. Reweighting

Reweighting is method to matchh the Monte Carlo data to the real detector data, to extract quantities not measurable by the detector like efficiencies. The match is done by applying weights to the Monte Carlo events.

As an initial weight the sWeights see equation 38 are used. he parameters used for reweighting are applied in the following order:

- number of tracks: 'nTracks'
- transversal momentum of the B Meson: ' $B p_T$ '
- quality of the $K\pi\mu\mu$ vertex.

The new weights derived by the difference in data and simulation of these parameters for the very clean channel $K^* \rightarrow J/\Psi K^*$ [20], are used to reweight the $B \rightarrow K^* \mu\mu$ Monte Carlo sample.

6.1. Results of the $B \rightarrow K^* \mu \mu$ reweighting

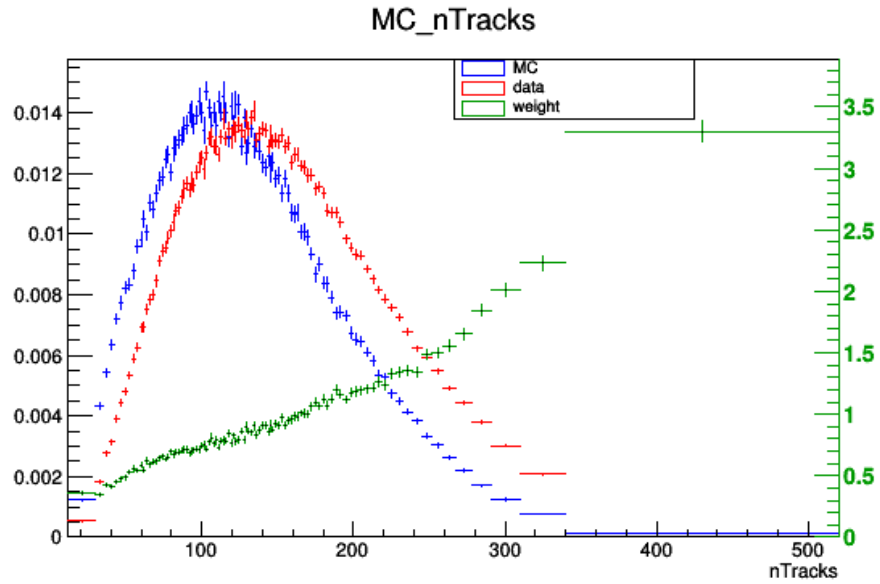


Figure 20: This plot shows the Monte Carlo Simulated data in blue, the detector data in red and in green the best weights to reweight the Monte Carlo data in order to match the detector data. The x- axes are the values for the number of tracks in an event (nTracks). On the left y-axes the fraction of events having nTracks is plotted. On the right y-axes the magnitude of the weights is shown.

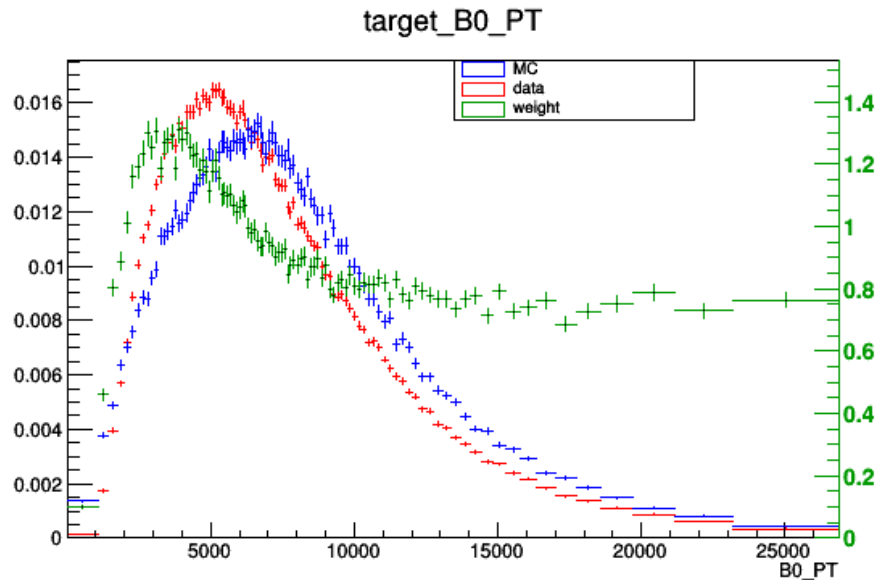


Figure 21: Same plot as in figure 20, for the transversal momentum of the B meson (B_0_{PT}) in MeV.

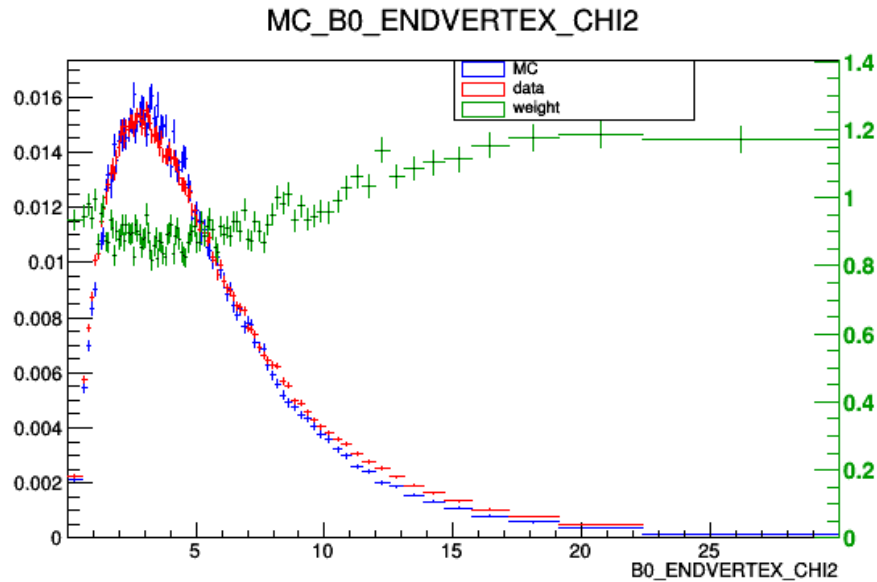


Figure 22: Same plot as in figure 20, for the quality of the $K\pi\mu\mu$ vertex ($B0_ENDVERTEX_CHI2$).

After applying those weights to the Monte Carlo data, the distributions of all the event parameters will change. To check if the simulation really matches the data. Some comparison plots have been made. One is presented here, while many others can be found in appendix C.

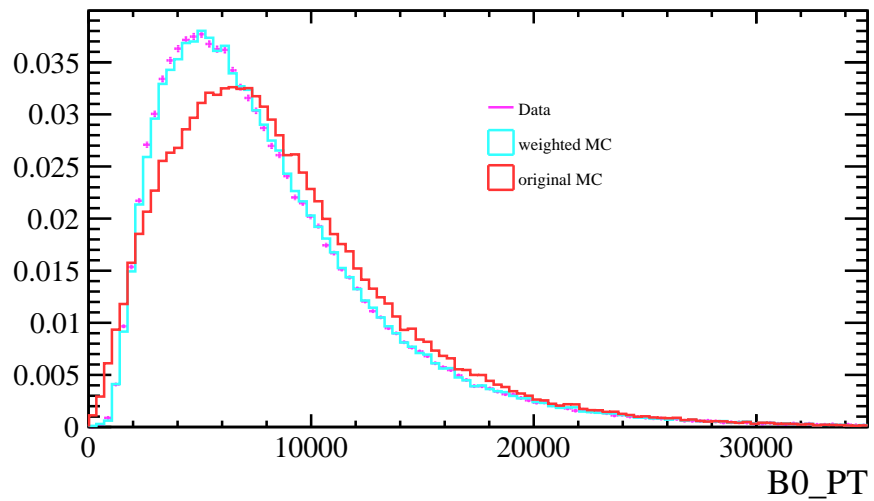


Figure 23: This plots shows the distribution of the B transversal momentum. The X achsis shows the B transversal momentum ($B0_PT$) in MeV. The violet points represent the distribution of ($B0_PT$) in the detector data. The red line represents the distribution of ($B0_PT$) before reweighting the Monte Carlo data. The blue line represents the distribution ($B0_PT$) after reweighting the Monte Carlo data.

6.2. SPlot

In this section the SPlot Technique is explained. It is used to separate two or more merged distributions and has been used to get the initial weights for the re-weighting in this chapter.

6.2.1. Likelihood method

Consider an analysis of a data sample, which consists of several types of events. These types represent signal components and background components, for example from different experiments. The log-likelihood of such a data sample is expressed as:

$$L = \sum_{i=1}^N \ln \left[\sum_{j=1}^{N_S} N_j f_j(y_i) \right] - \sum_{i=1}^{N_S} N_j \quad (19)$$

- N = total number of events
- N_S = number of types
- N_i = expected average number of events for type i
- y = set of discriminating variables
- f_j = PDF of the i th type
- $f_j(y_i)$ = value of PDF for event y_i
- x = control variable, not a part of L by construction

The yields N_i and the free parameters of the PDF are obtained by maximizing the above log-likelihood (eq 19).

6.2.2. *inPlot* technique

Consider a variable x which can be expressed as a function of the discriminating variables y used in the fit. Furthermore a fit has been performed to determine the yields N_i for all types. From the knowledge of the PDF and the values of N_i a naive weight can be defined as:

$$P_n(y_i) = \frac{N_n f_n(y_i)}{\sum_{k=1}^{N_S} N_k f_k(y_i)} \quad (20)$$

Therefore $N_n \tilde{M}_n(\bar{x})$ is the x -distribution of the plotted events, using the weights of eq 20.

$$N_n \tilde{M}_n(\bar{x}) = \sum_{i \subset \delta x} P_n(y_i) \quad (21)$$

where sum $\sum_{i \subset \delta x}$ contains all events for which x_i lies in the interval centered on \bar{x} and of total width δx . Therefore $N_n \tilde{M}_n(\bar{x}) \delta x$ is the x -distribution of the histogrammed events, using the weights of eq 20.

With this procedure one can on average reproduce the true distribution $\mathbf{M}_n(x)$. One can even replace the sum in eq 21 by an integral:

$$\left\langle \sum_{i \in \delta x} \right\rangle \rightarrow \int dy \sum_{j=1}^{N_s} N_j f_j(y) \delta(x(y) - \bar{x}) \delta x \quad (22)$$

Furthermore through identifying the number of events N_i from the fit one gets:

$$\langle N_n \rangle \tilde{M}_n(\bar{x}) = \int dy \sum_{j=1}^{N_s} N_j f_j(y) \delta(x(y) - \bar{x}) P_n(y) \quad (23)$$

$$= \int dy \sum_{j=1}^{N_s} N_j f_j(y) \delta(x(y) - \bar{x}) \cdot \frac{N_n f_n(y)}{\sum_{k=1}^{N_s} N_k f_k(y)} \quad (24)$$

$$= N_n \int dy \delta(x(y) - \bar{x}) f_n(y) \quad (25)$$

$$= N_n \mathbf{M}_n(\bar{x}) \quad (26)$$

One can see that the sum over events of the naive weight P_n provides a direct estimate of the x-distribution for the nth type. But this procedure has a major drawback. Since x is correlated to y, the PDFs of x enter implicitly in the definition of the naive weight. Therefore the \tilde{M}_n distributions are a bad estimate for the quality of the fit. These distributions are biased in a difficult way, when the PDFs $f_i(y)$ are not accurate.

Consider for example a data sample where one of the types has events on the tail of the x-distribution. Such events require the true distribution to account for the tail. But since the events are averaged the weights on the tail are going to be very small missing those events in the estimated true distribution. Only the core of the x-distribution can be examined with *in Plots*.

6.2.3. s Plot technique

In the previous section it was shown that if a variable x belongs to a set y of discriminating variables, the expected x distribution can be reconstructed. Consider now two sets of variables x and y , where x does not belong to y and which are uncorrelated, hence the total PDFs $f_i(x, y)$ all factorize into products $\mathbf{M}_i(x) f_i(y)$. The equation 26 does not hold anymore because, when summing over the events the x-PDFs $\mathbf{M}_j(x)$ appear:

$$\langle N_n \rangle \tilde{M}_n(\bar{x}) = \int \int dy dx \sum_{j=1}^{N_s} N_j \mathbf{M}_j(x) f_j(y) \delta(x - \bar{x}) P_n \quad (27)$$

$$= \int dy \sum_{j=1}^{N_s} N_j \mathbf{M}_j(\bar{x}) f_j(y) \frac{N_n f_n(y)}{\sum_{k=1}^{N_s} N_k f_k(y)} \quad (28)$$

$$= N_n \sum_{j=1}^{N_s} \mathbf{M}_j(\bar{x}) \left(N_j \int dy \frac{f_n(y) f_j(y)}{\sum_{k=1}^{N_s} N_k f_k(y)} \right) \quad (29)$$

$$\neq N_n \mathbf{M}_n(\bar{x}). \quad (30)$$

The correction term

$$N_j \int dy \frac{f_n(y) f_j(y)}{\sum_{k=1}^{N_s} N_k f_k(y)} \quad (31)$$

is not identical to the kroenecker delta δ_{jn} . In fact the $N_n \tilde{M}_n$ distribution obtained by the naive weight is a linear combination of the true distribution \mathbf{M}_j .

To go forward one has to realize that the correction term is related to the inverse of the covariance matrix, given by the second derivatives of $-L$, after the minimization.

$$\mathbf{V}_{nj}^{-1} = \frac{\partial^2(-L)}{\partial N_n \partial N_j} = \sum_{i=1}^N \frac{f_n(y_i) f_j(y_i)}{\left(\sum_{k=1}^{N_s} N_k f_k(y_i) \right)^2} \quad (32)$$

If one averages and is replacing the sum over events by intergals (eq 22) the varaince matrix reads:

$$\langle \mathbf{V}_{nj}^{-1} \rangle = \int \int dy dx \sum_{e=1}^{N_s} N_e \mathbf{M}_e(x) f_e(y) \frac{f_n(y) f_j(y)}{\left(\sum_{k=1}^{N_s} N_k f_k(y) \right)^2} \quad (33)$$

$$= \int dy \sum_{e=1}^{N_s} N_e f_e(y) \frac{f_n(y) f_j(y)}{\left(\sum_{k=1}^{N_s} N_k f_k(y) \right)^2} \cdot \int dx \mathbf{M}_l(x) \quad (34)$$

$$= \int dy \frac{f_n(y) f_j(y)}{\sum_{k=1}^{N_s} N_k f_k(y)} \quad (35)$$

Therefor equation 27 can be rewritten as:

$$\langle \tilde{M}_n(\bar{x}) \rangle = \sum_{j=1}^{N_s} \mathbf{M}_j(\bar{x}) N_j \langle \mathbf{V}_{nj}^{-1} \rangle. \quad (36)$$

To get the distribution of intrest one has to invert this matrix equation:

$$N_n \mathbf{M}_n(\bar{x}) = \sum_{j=1}^{N_s} \langle \mathbf{V}_{nj} \rangle \langle \tilde{M}_j(\bar{x}) \rangle \quad (37)$$

The true distribution of x can still be reconstructed using the naive weight (eq 20), through a linear combination of *sPlots*. In other words: When x does not belong to the set y , the weights are not given by equation 20, they are given by a covariance-weighted quantity called *sWeight* defined by:

$${}_s P_n(y_i) = \frac{\sum_{j=1}^{N_s} \mathbf{V}_{nj} f_j(y_i)}{\sum_{k=1}^{N_s} N_k f_k(y_i)} \quad (38)$$

With the *sWeights* on can obtain the distribution of the x variable by histogramming the *sPlot*:

$$N_{ns} \tilde{M}_n(\bar{x}) \delta x = \sum_{i \subset \delta x} {}_s P_n(y_i) \quad (39)$$

On average it reproduced the true distribution:

$$\langle N_{ns} \tilde{M}_n(x) \rangle = N_n \mathbf{M}_n(x) \quad (40)$$

In the case were x is significantly correlated with y , the *sPlots* from equation 39 can not be compared with the pure distributions of the various types. To solve that problem one can perform a Monte Carlo simulation of the procedure and obtain the expected distributions to which the *sPlots* should be compared.

More information on *sPlots* is given in reference [21].

7. Outlook

The RooMCMMarkovChain fitting routine is currently being added [22] to the ROOT Data analysis framework. The best classifier uBoost from the classifiers test will be used to find future $B \rightarrow K^* \mu\mu$ decays in the data produced by the LHCb detector. The reweighting done in this thesis will be used for the future analysis of the $B \rightarrow K^* \mu\mu$ in the current LHCb data.

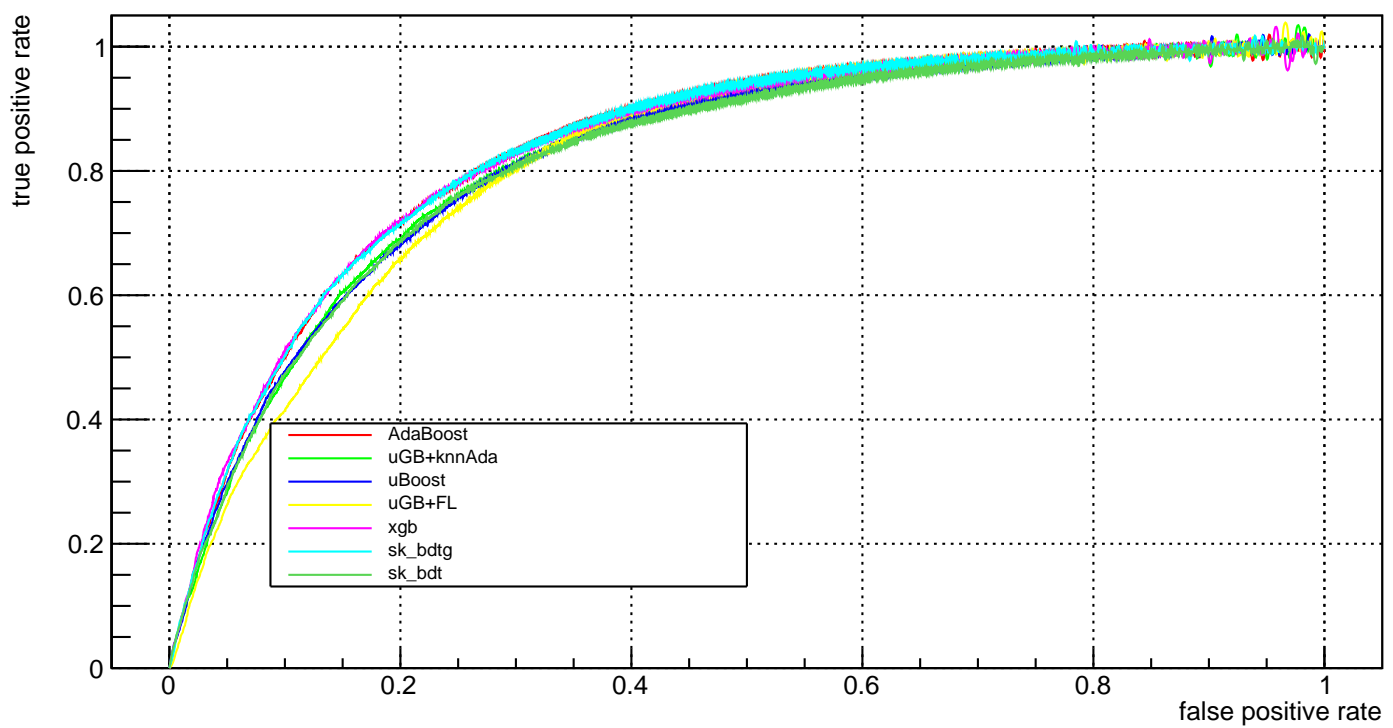
References

- [1] ROOT Data Analysis Framework <https://root.cern.ch/>
- [2] MINUIT Home page, <https://seal.web.cern.ch/seal/snapshot/work-packages/mathlibs/minuit/>
- [3] JHEP08 (2017) 055
- [4] C. Bobeth, M. Misiak and J. Urban, Nucl. Phys. B 574 (2000) 291 [arXiv:hep-ph/9910220].
- [5] arXiv:0811.1214 [hep-ph]
- [6] CERN Accelerator Complex, <http://www.stfc.ac.uk/research/particle-physics-and-particle-astrophysics/large-hadron-collider/cern-accelerator-complex/>
- [7] Science and Technology Facilities Council article about LHCb , <https://www.ppd.stfc.ac.uk/Pages/LHCb.aspx>
- [8] VELO description, <http://lhcb-public.web.cern.ch/lhcb-public/en/Detector/VELO2-en.html>
- [9] RICH description, <http://lhcb-public.web.cern.ch/lhcb-public/en/Detector/RICH2-en.html>
- [10] Magnet description, <http://lhcb-public.web.cern.ch/lhcb-public/en/Detector/Magnet2-en.html>
- [11] Tracker description, <http://lhcb-public.web.cern.ch/lhcb-public/en/Detector/Trackers2-en.html>
- [12] Calorimeters description, <http://lhcb-public.web.cern.ch/lhcb-public/en/Detector/Calorimeters2-en.html>
- [13] Muon system description, <http://lhcb-public.web.cern.ch/lhcb-public/en/Detector/Muon2-en.html>
- [14] A Short Introduction to Boosting, by Yoav Freund and Robert E. Schapire <http://www.csie.ntu.edu.tw/~stan/csi5387/boost-tut-ppr.pdf>
- [15] J.H. Friedman, "Greedy function approximation: A gradient boosting machine", 2001
- [16] J. Stevens and M. Williams, uBoost: A boosting method for producing uniform selection efficiencies from multivariate classifiers, JINST 8, P12013 (2013). [arXiv:1305.7248]
- [17] arXiv:1603.02754 [cs.LG]
- [18] Gradient Boosting classifier from the sk_learn python package <http://scikit-learn.org/stable/modules/generated/sklearn.ensemble.GradientBoostingClassifier.html>
- [19] A variation of the AdaBoost classifier called AdaBoost-SAMME <http://scikit-learn.org/stable/modules/generated/sklearn.ensemble.AdaBoostClassifier.html>
- [20] <https://arxiv.org/pdf/1103.0423.pdf>

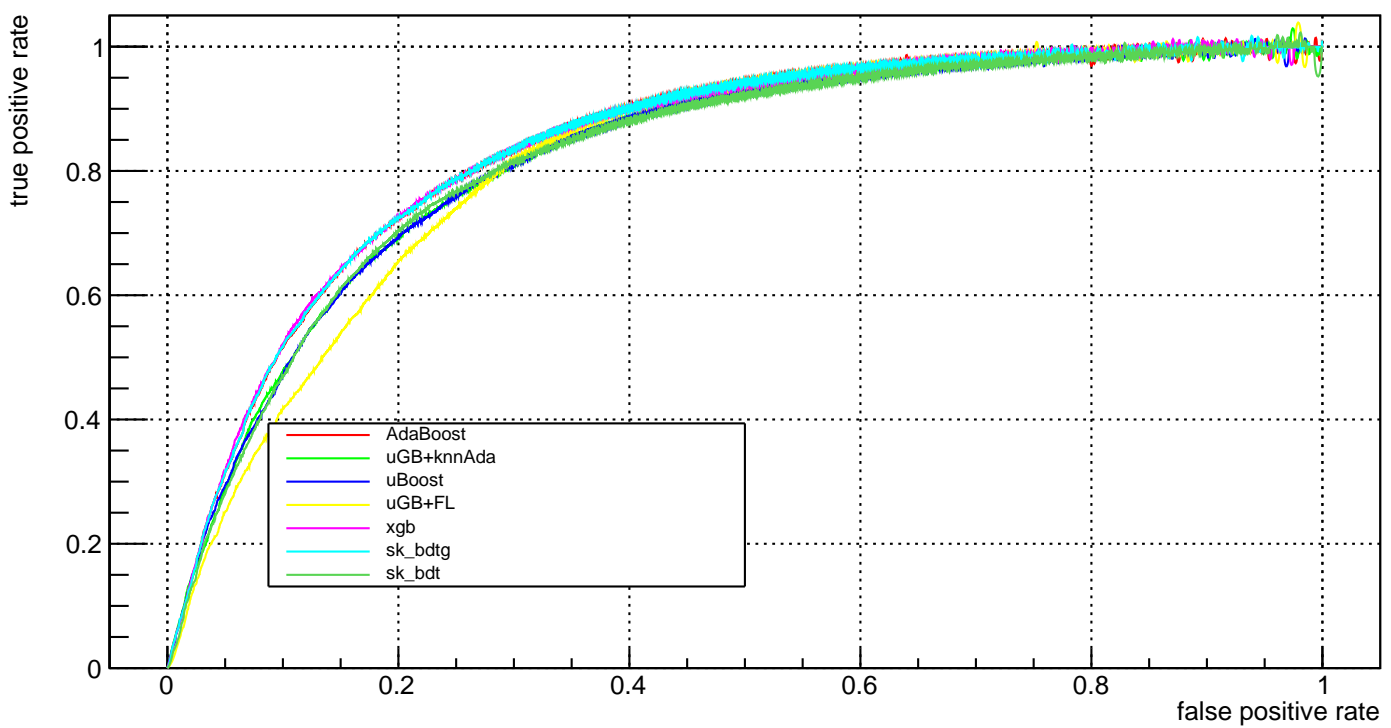
- [21] sPlot: a statistical tool to unfold data distributions, arXiv:physics/0402083 [physics.data-an]
- [22] <https://github.com/root-project/root/pull/1422>

A. ROC curves

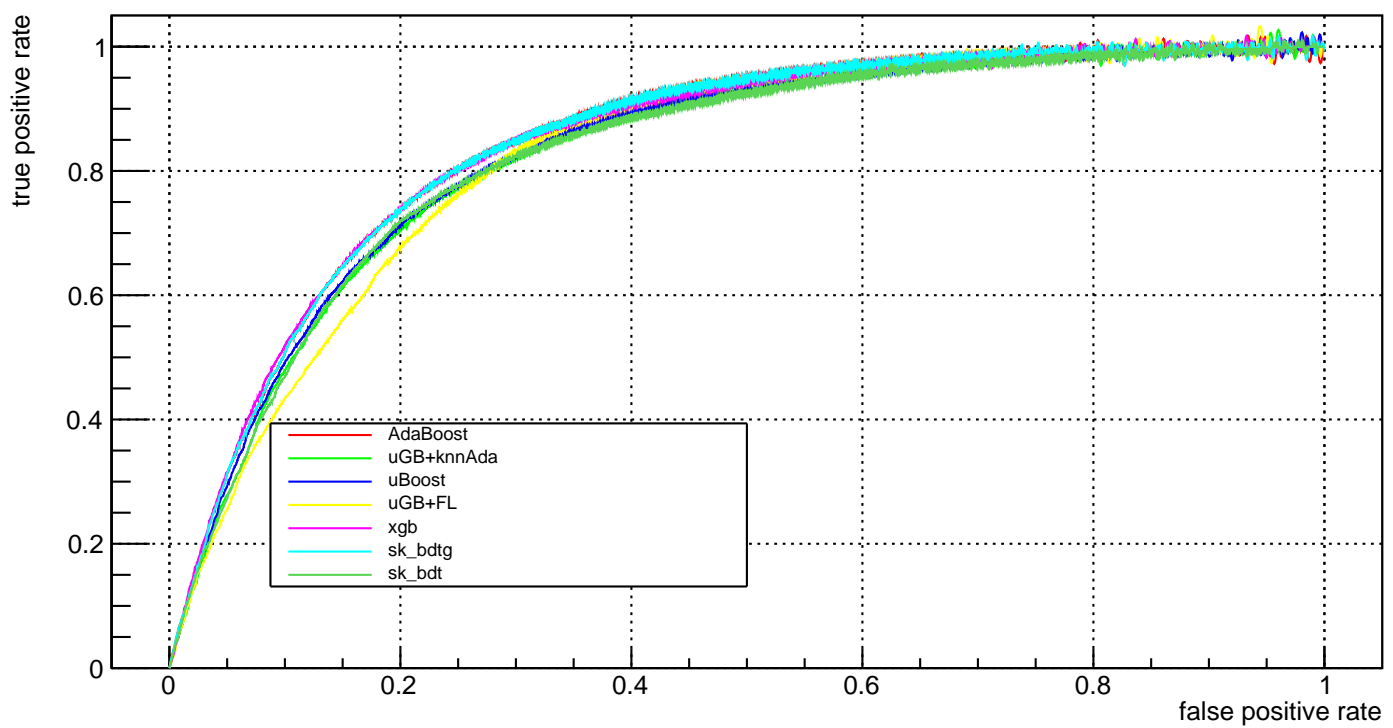
fold_0_roc



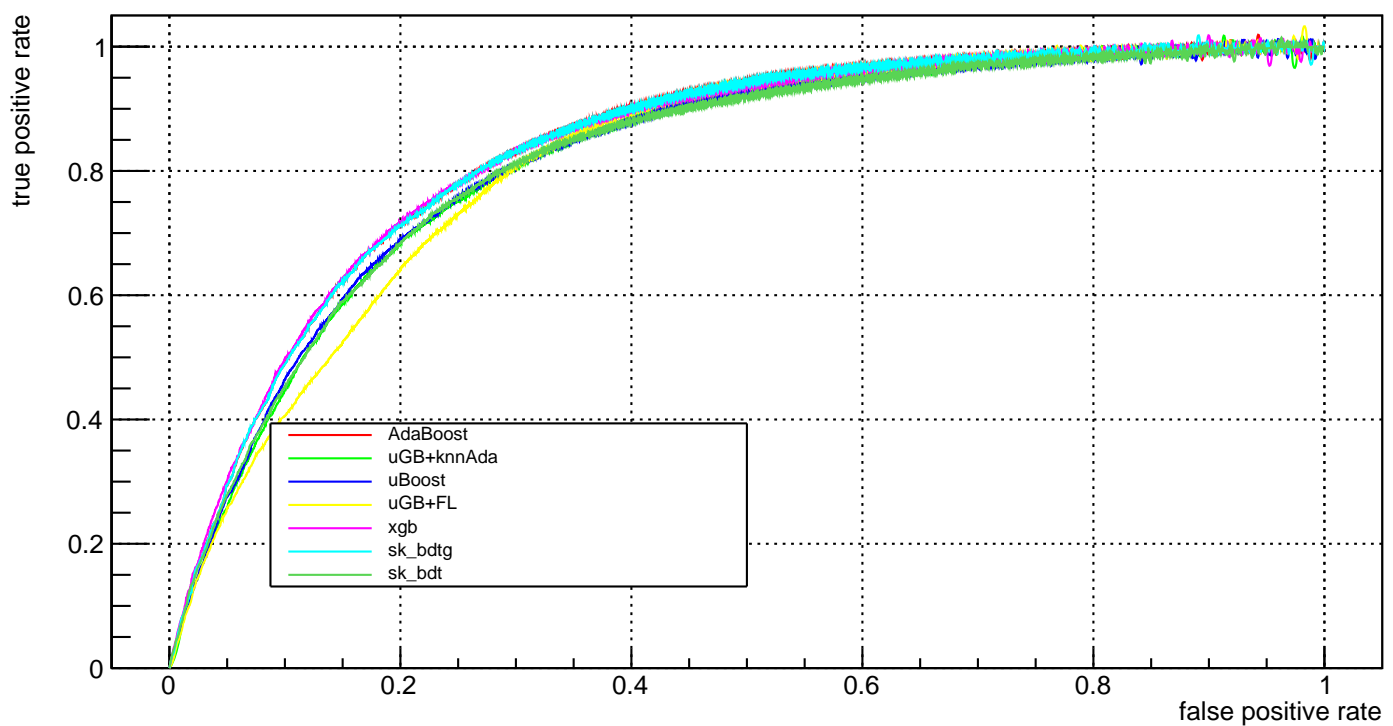
fold_1_roc



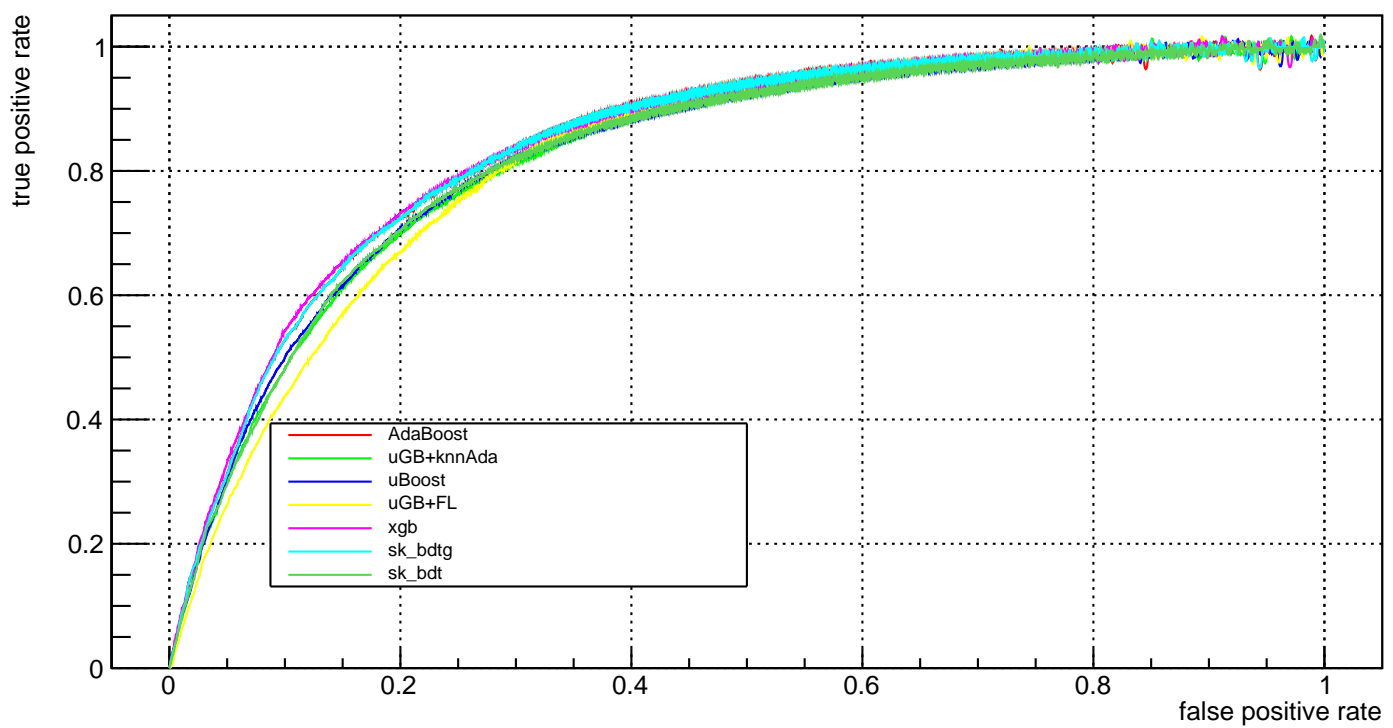
fold_2_roc



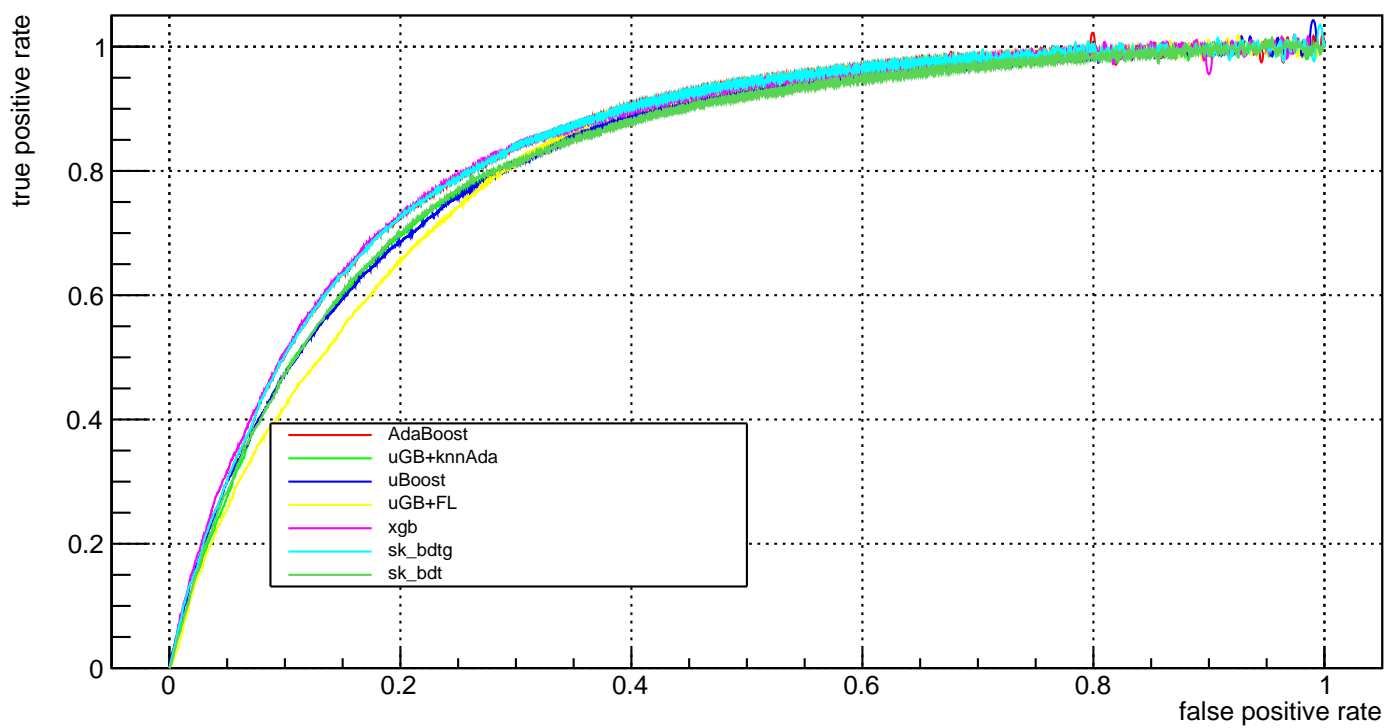
fold_3_roc



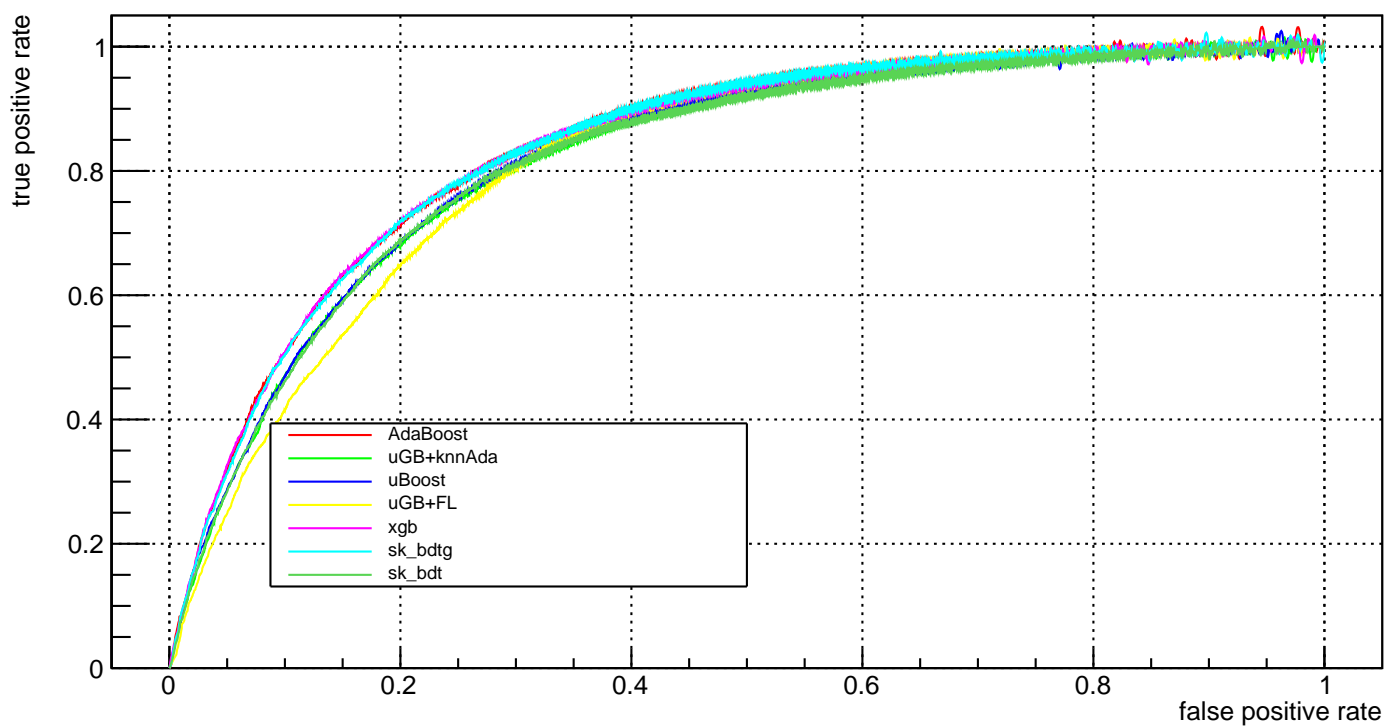
fold_4_roc



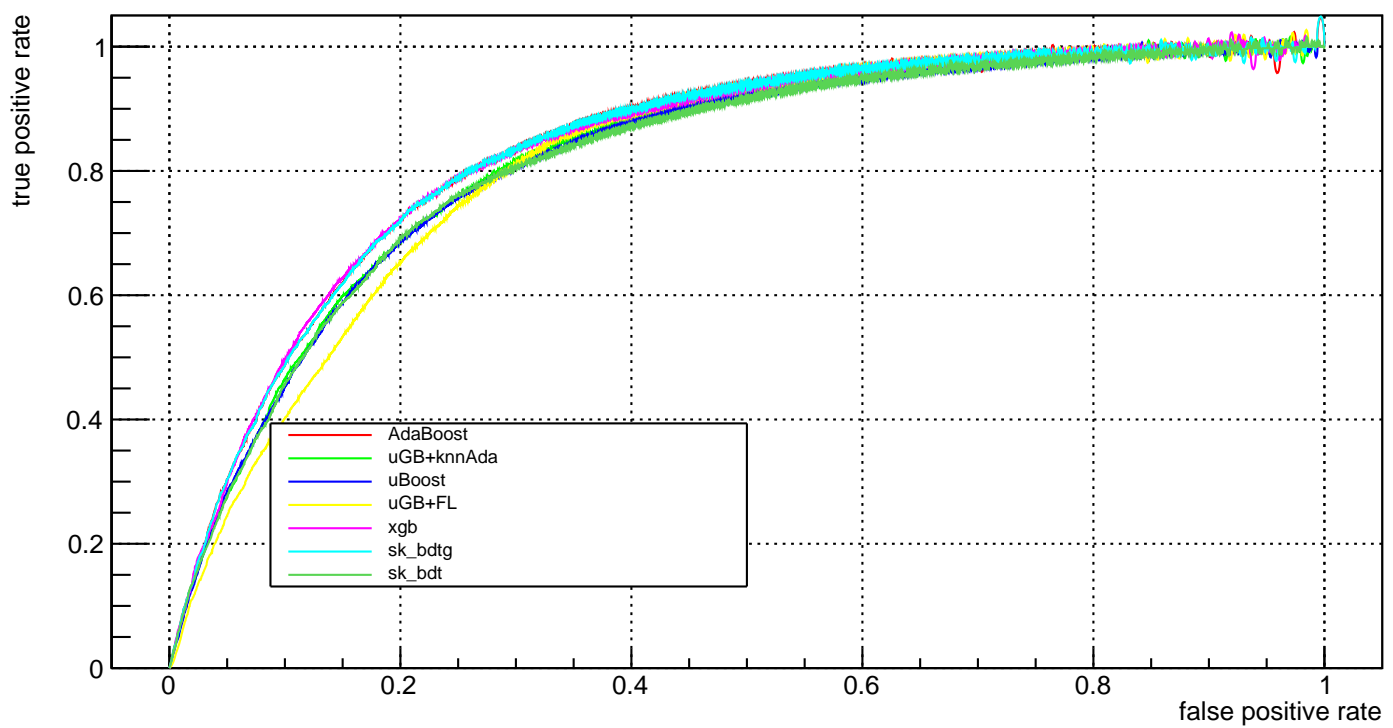
fold_5_roc



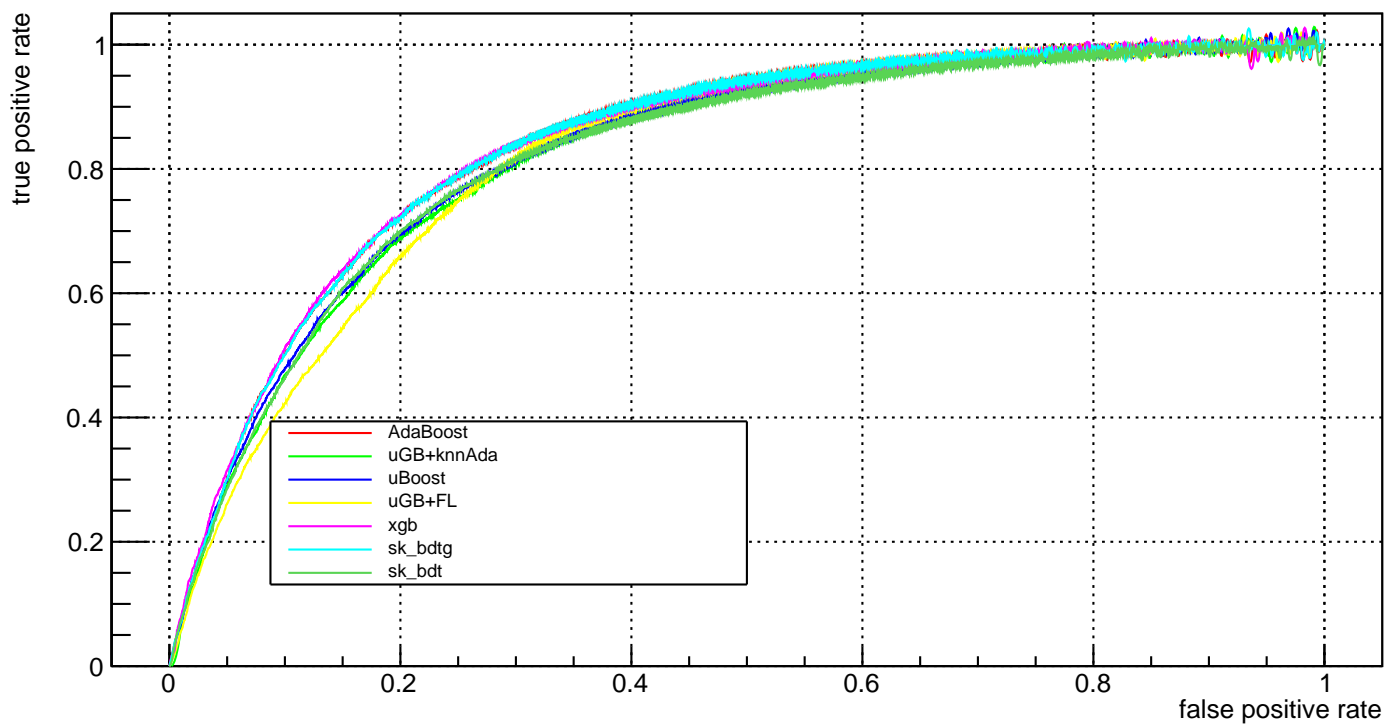
fold_6_roc



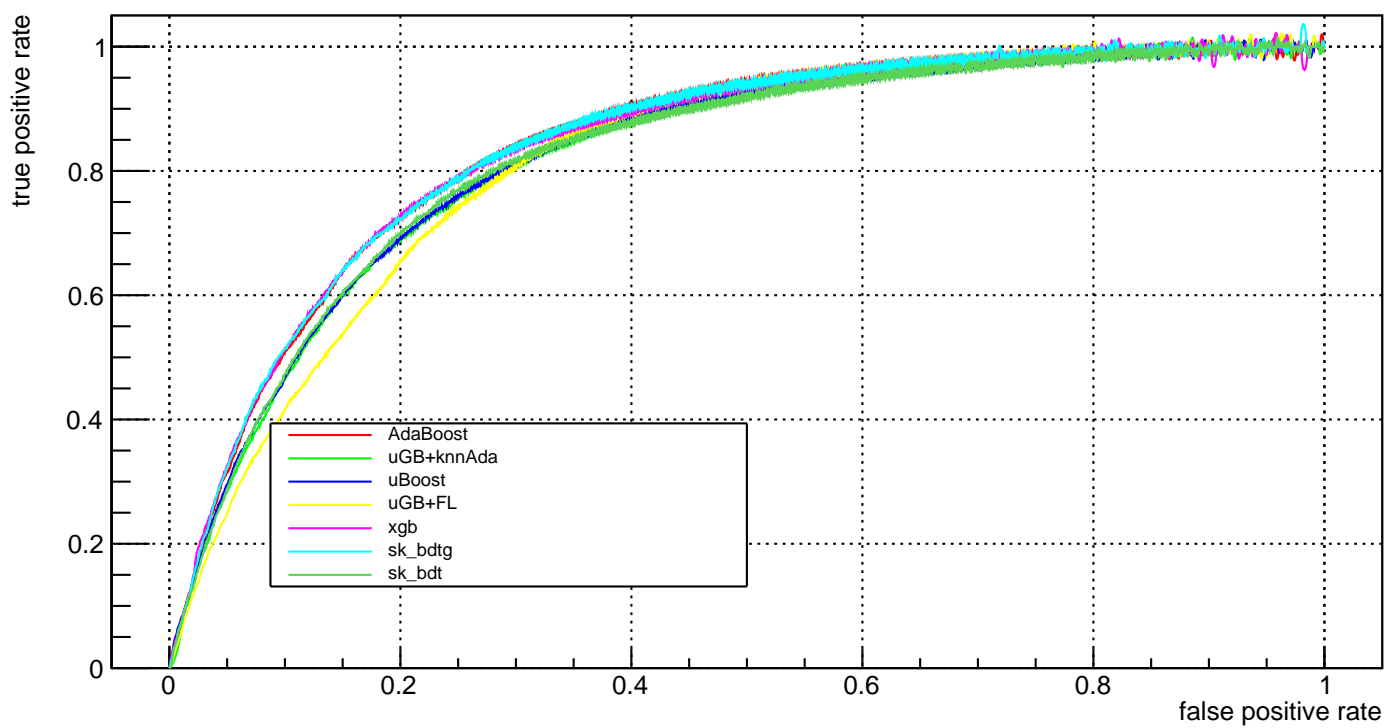
fold_7_roc



fold_8_roc

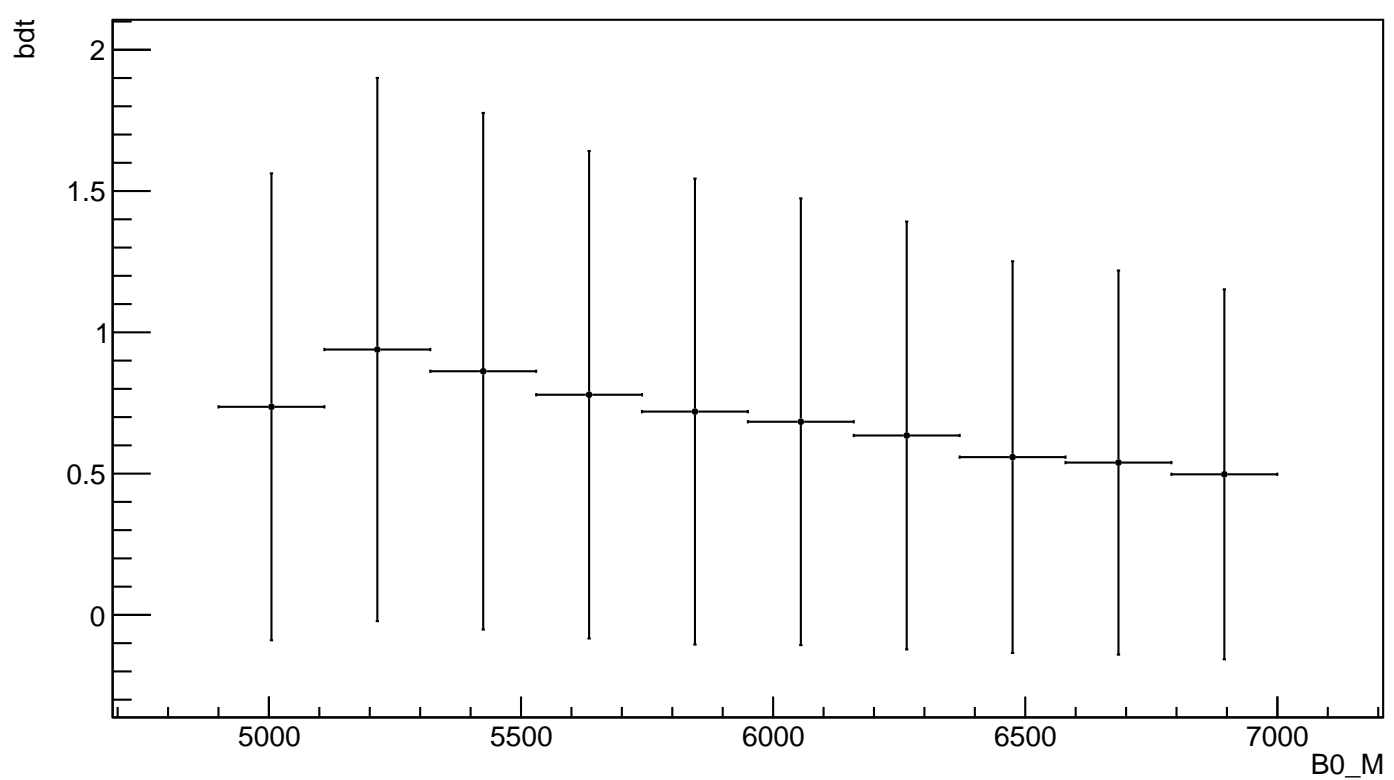


fold_9_roc

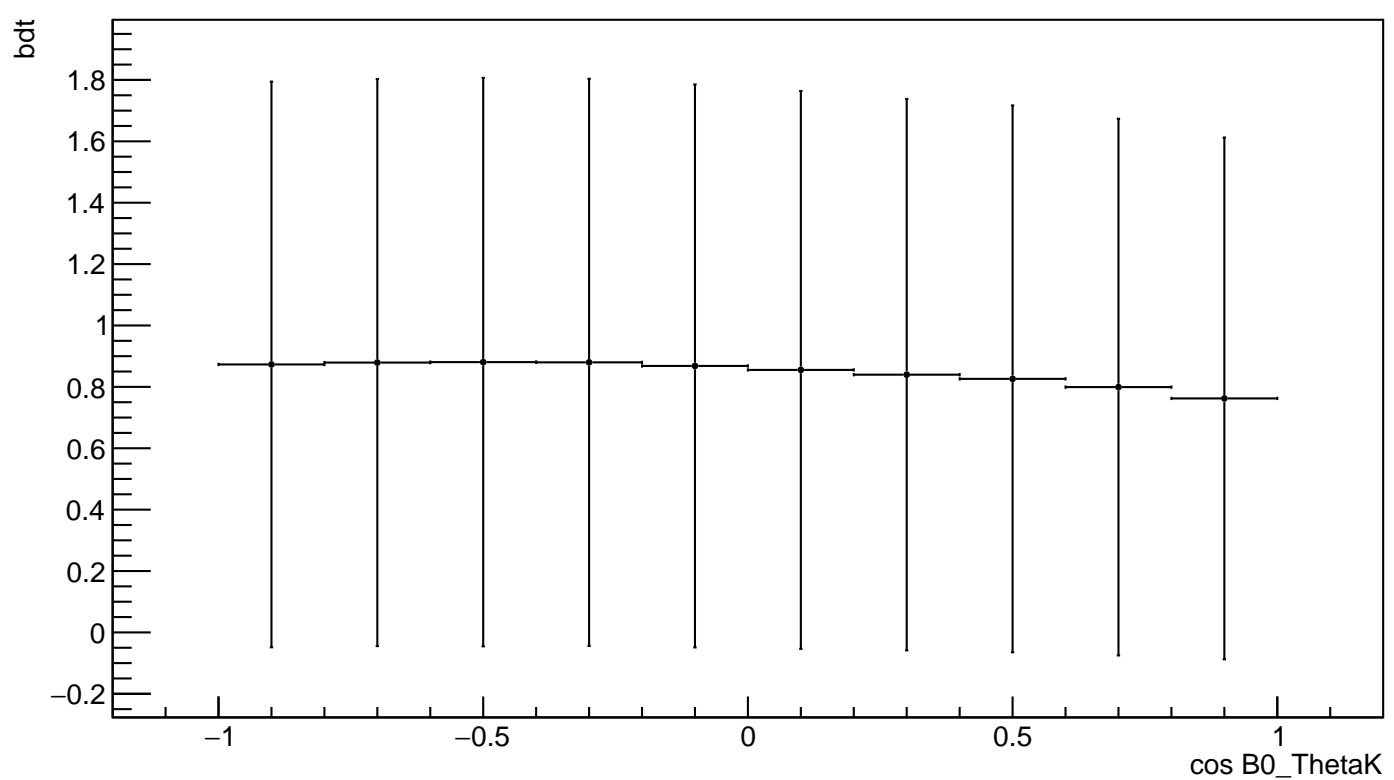


B. Correlation plots

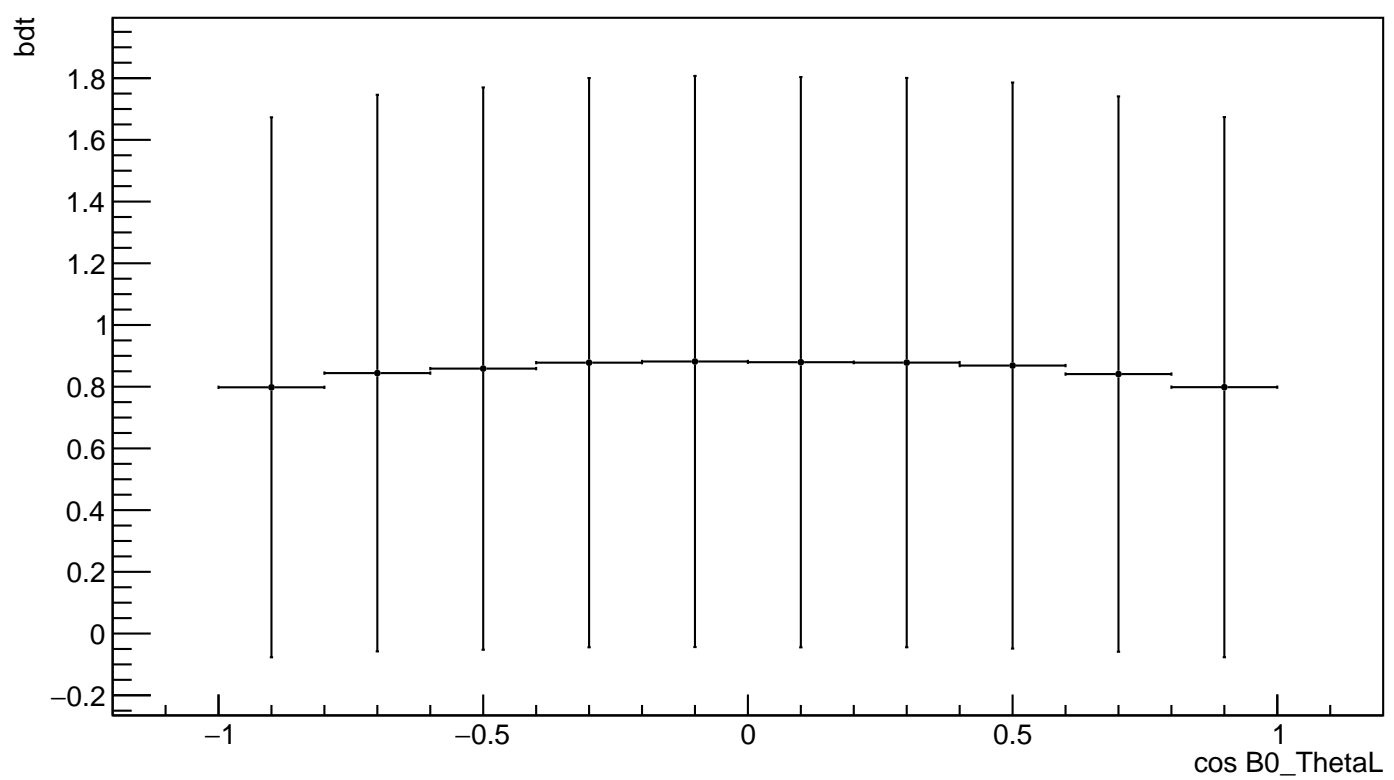
AdaBoost_plot_bdt_vs_B0_M



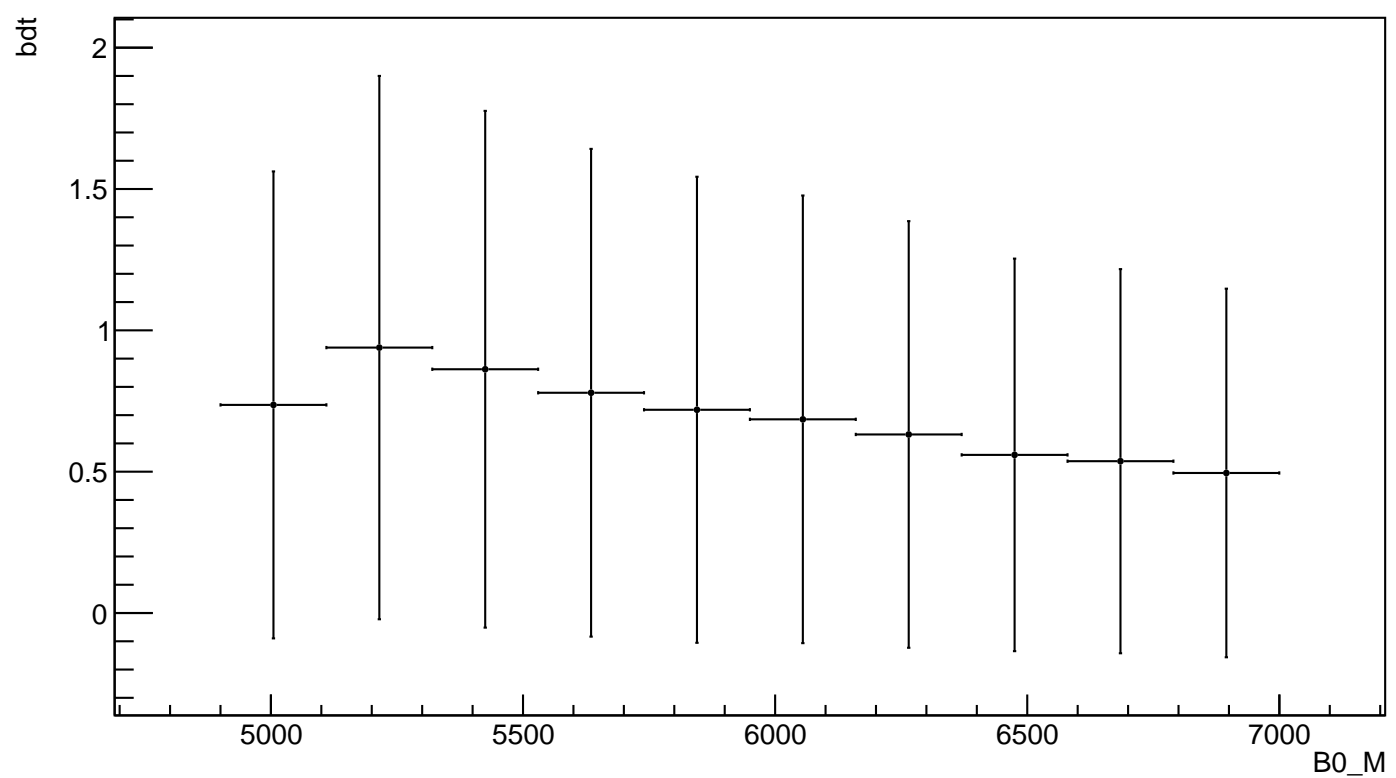
AdaBoost_plot_bdt_vs_B0_ThetaK



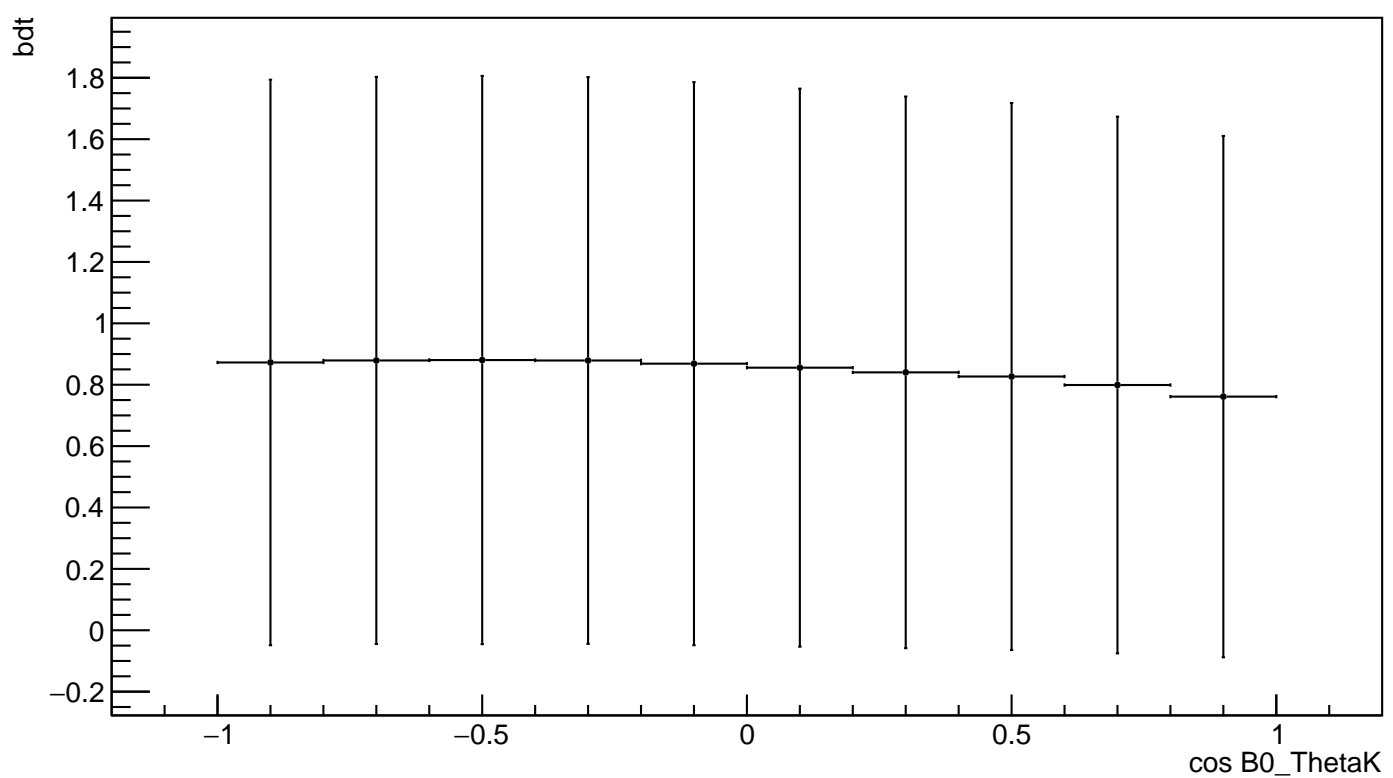
AdaBoost_plot_bdt_vs_B0_ThetaL



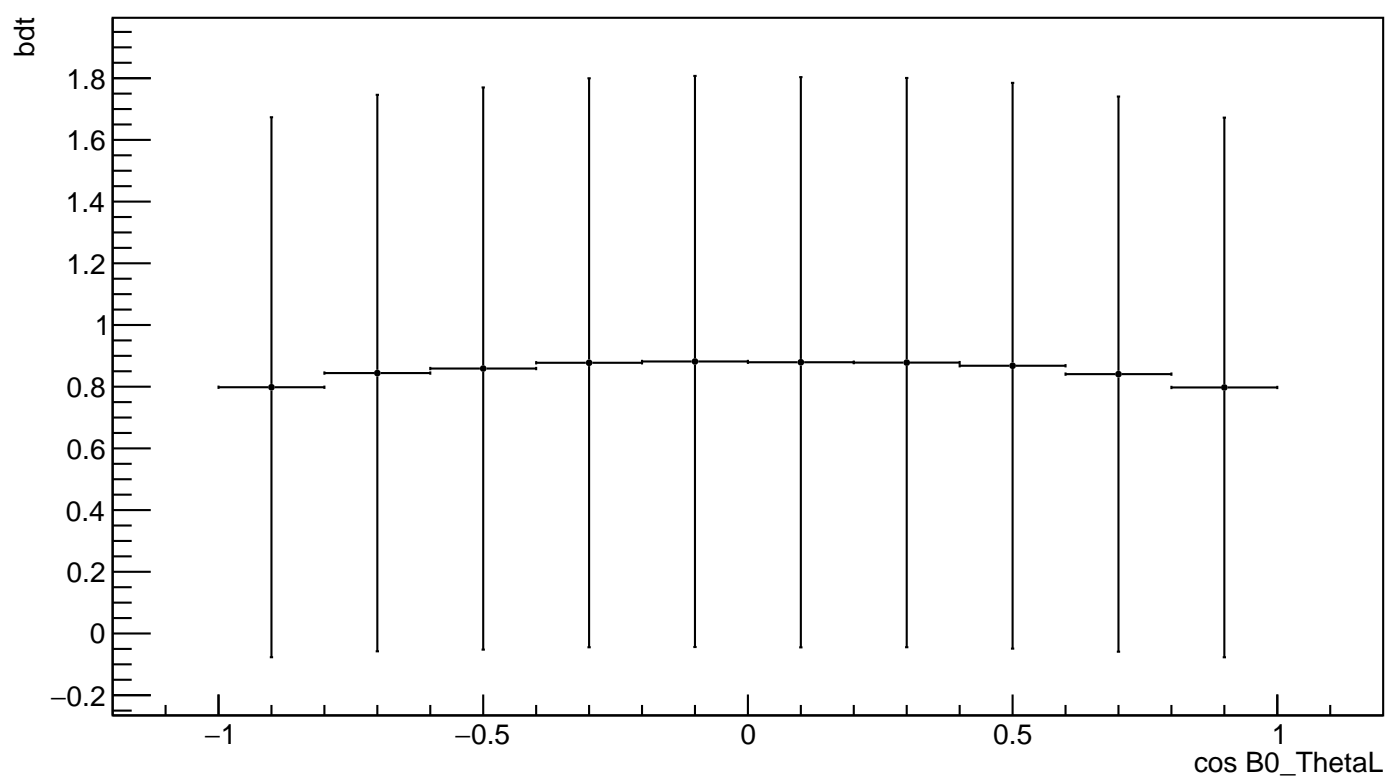
sk_bdtg_plot_bdt_vs_B0_M



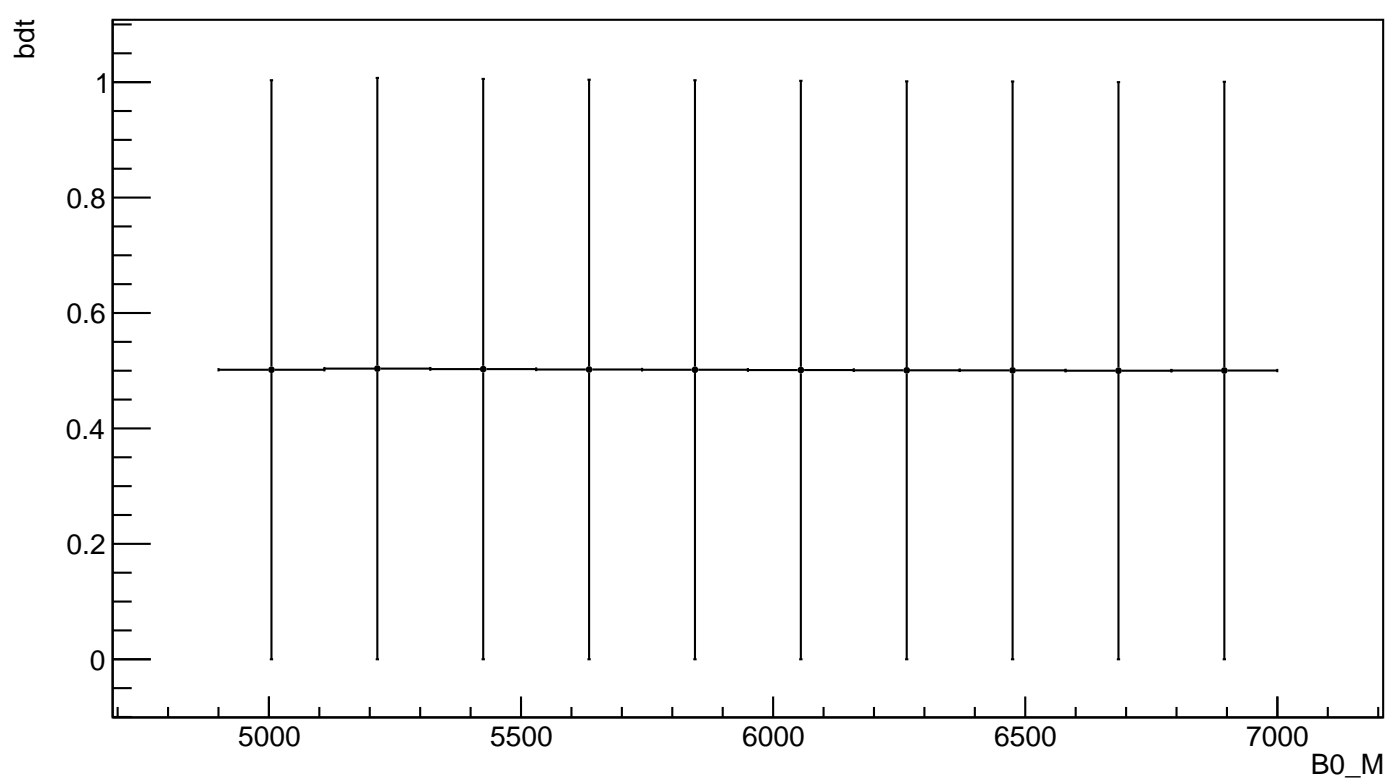
sk_bdtg_plot_bdt_vs_B0_ThetaK



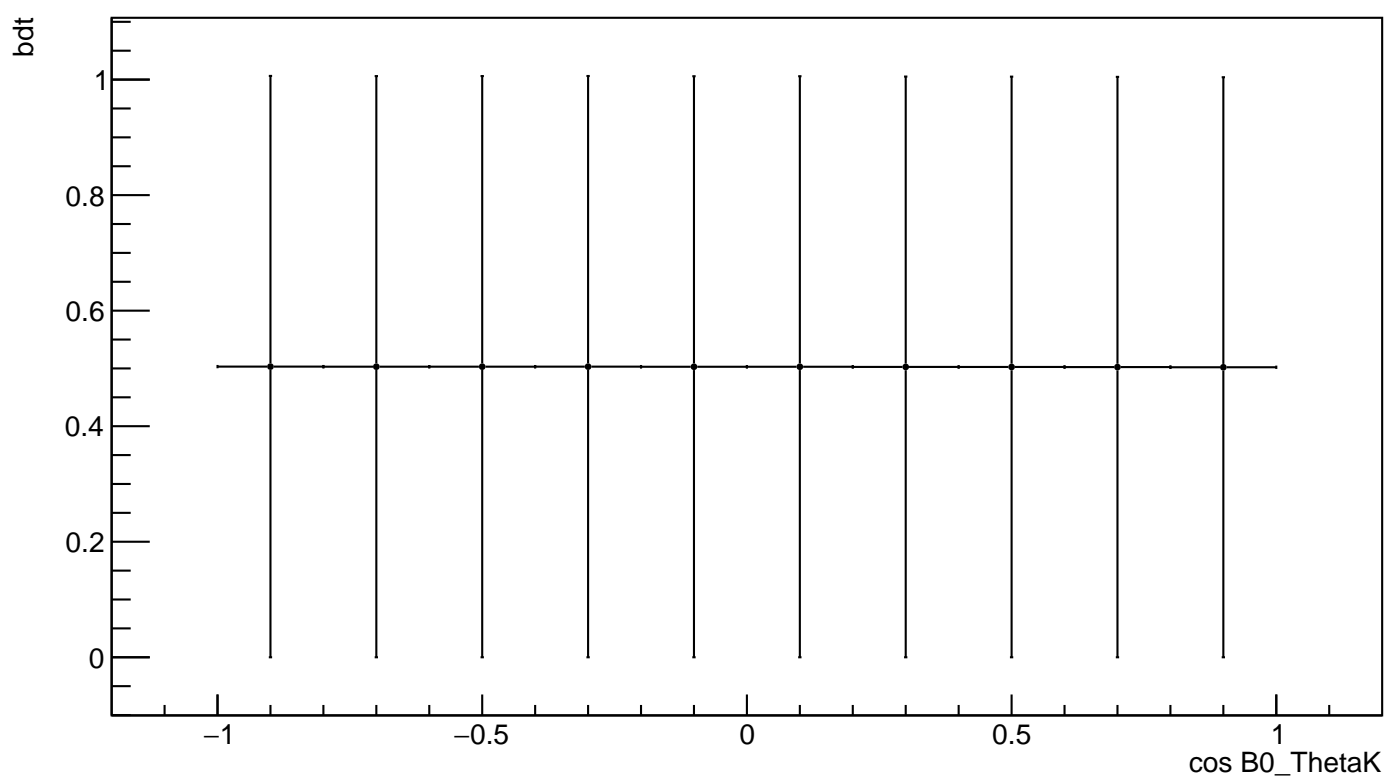
sk_bdtg_plot_bdt_vs_B0_ThetaL



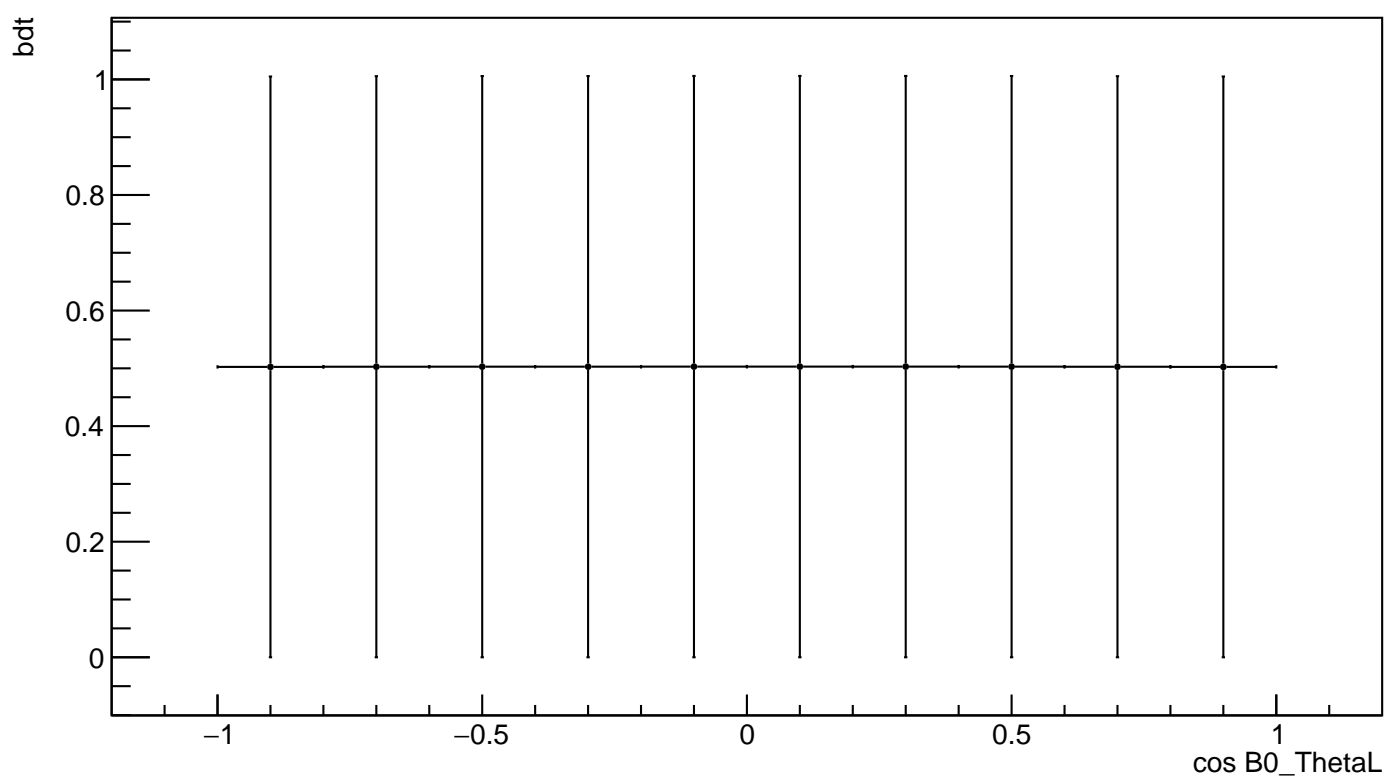
sk_bdt_plot_bdt_vs_B0_M



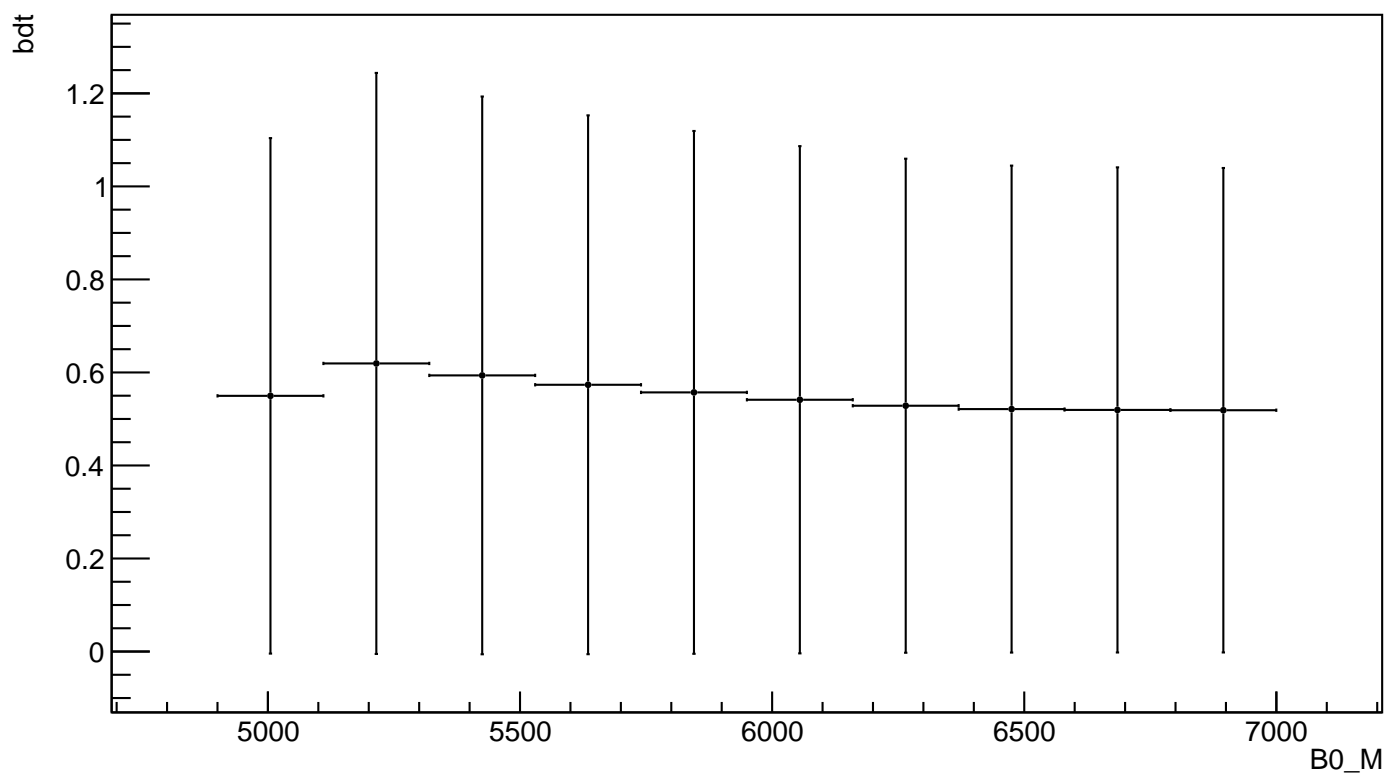
sk_bdt_plot_bdt_vs_B0_ThetaK



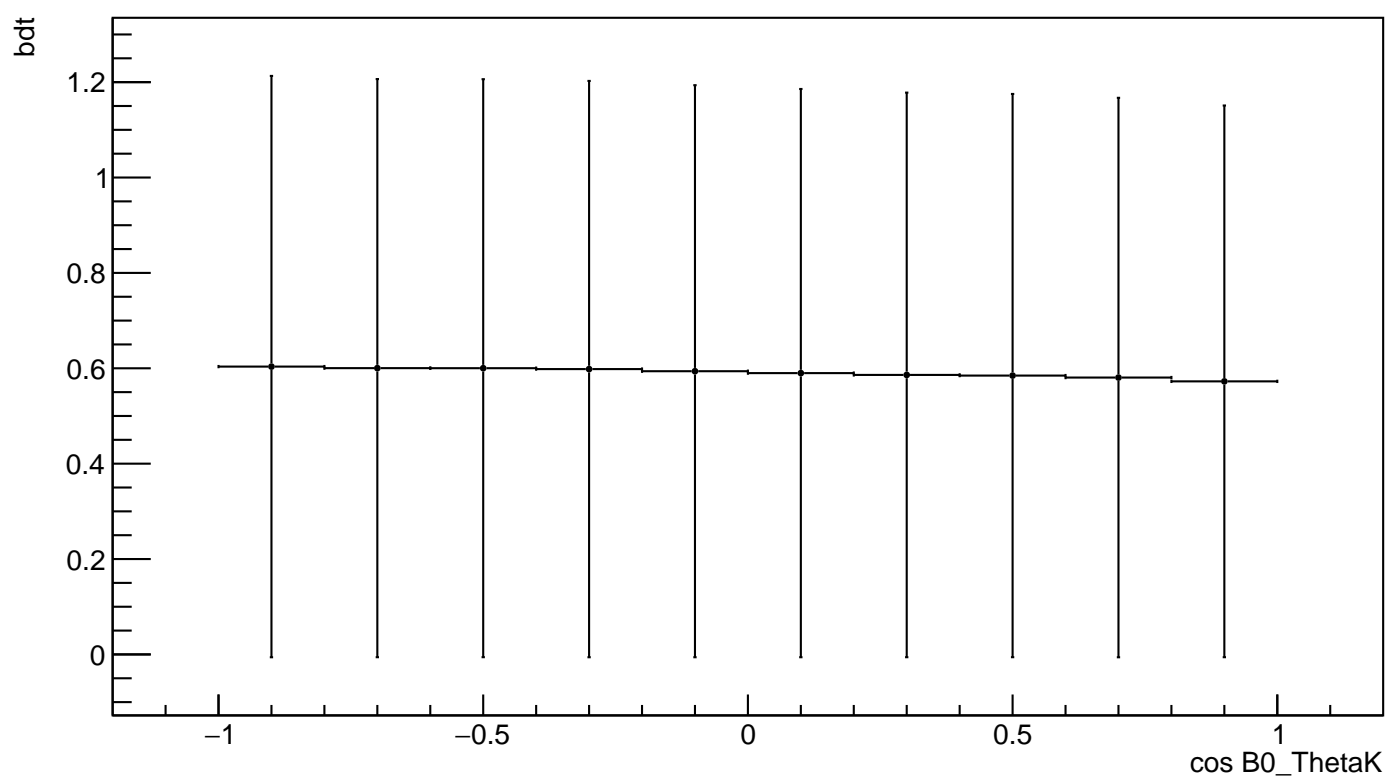
sk_bdt_plot_bdt_vs_B0_ThetaL



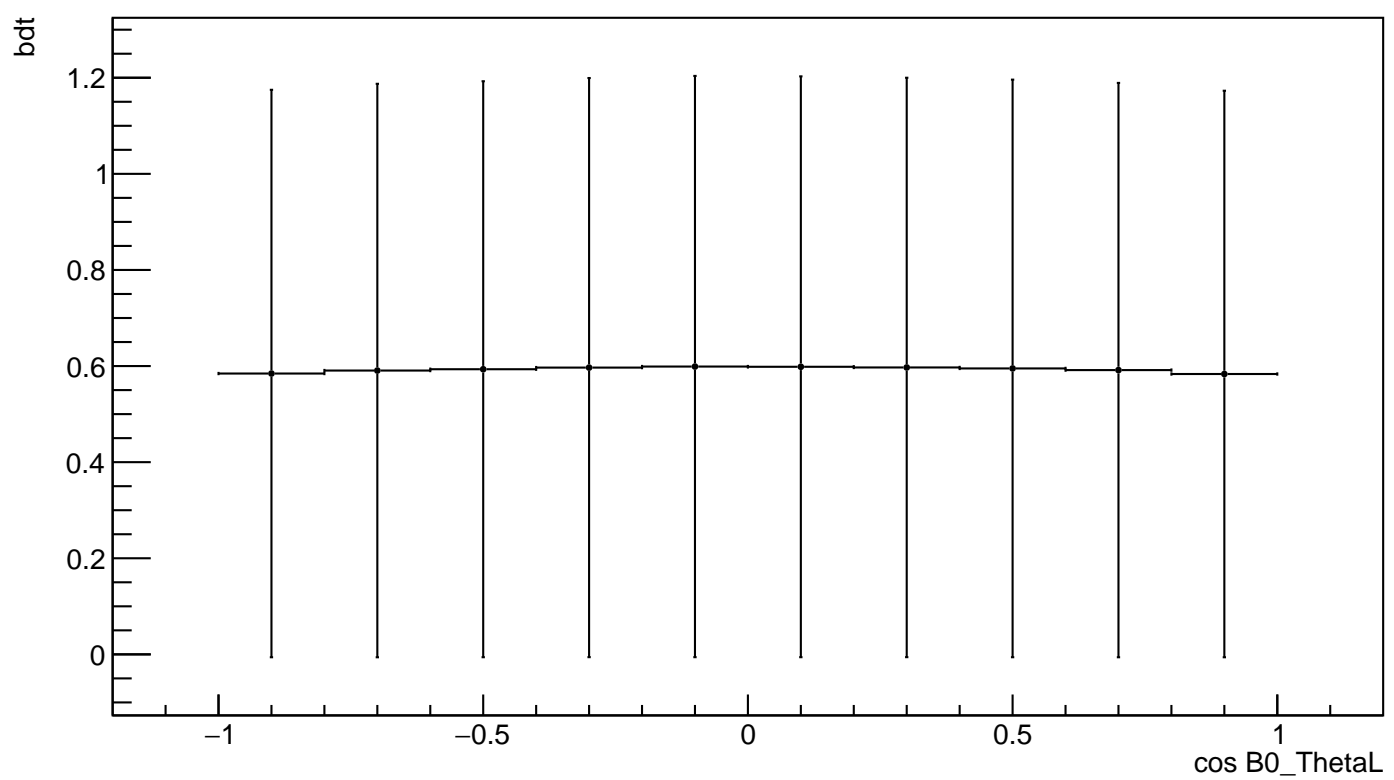
uBoost_plot_bdt_vs_B0_M



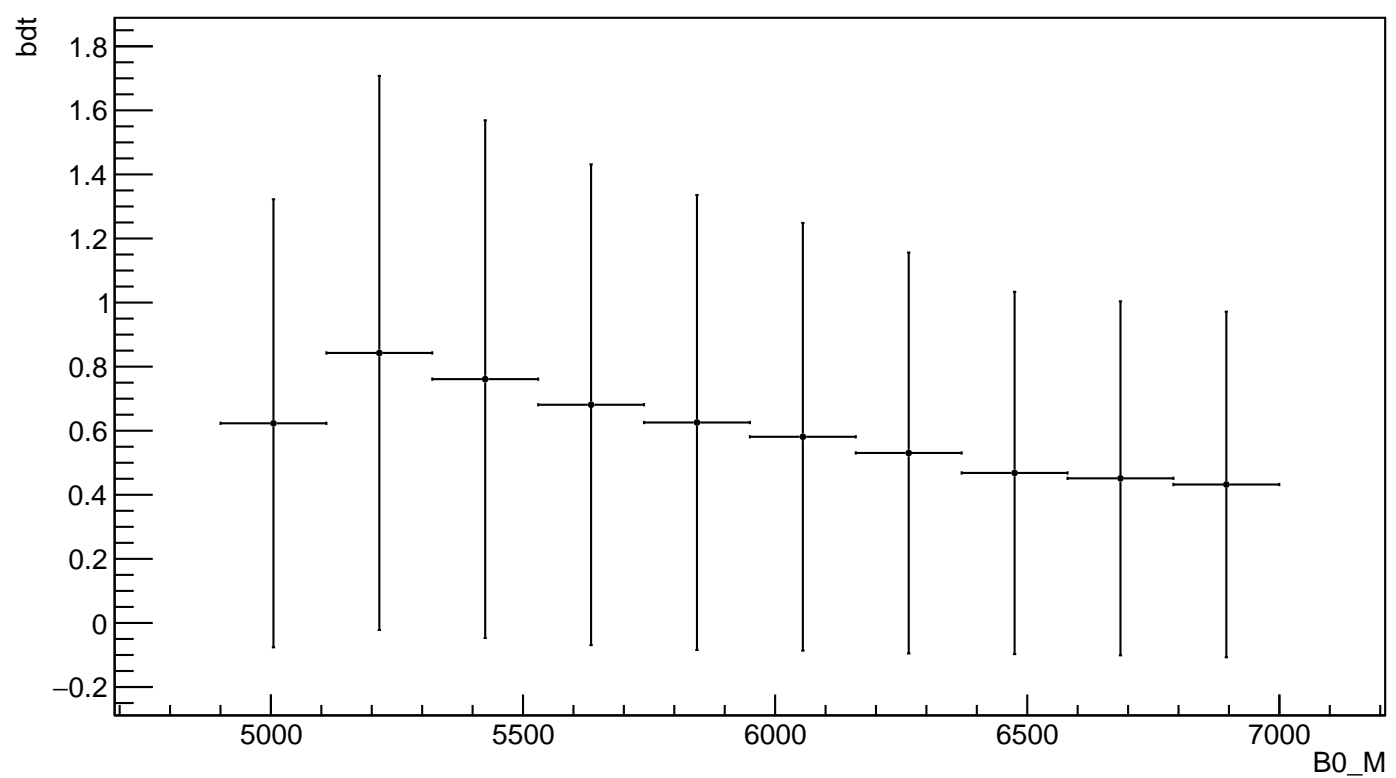
uBoost_plot_bdt_vs_B0_ThetaK



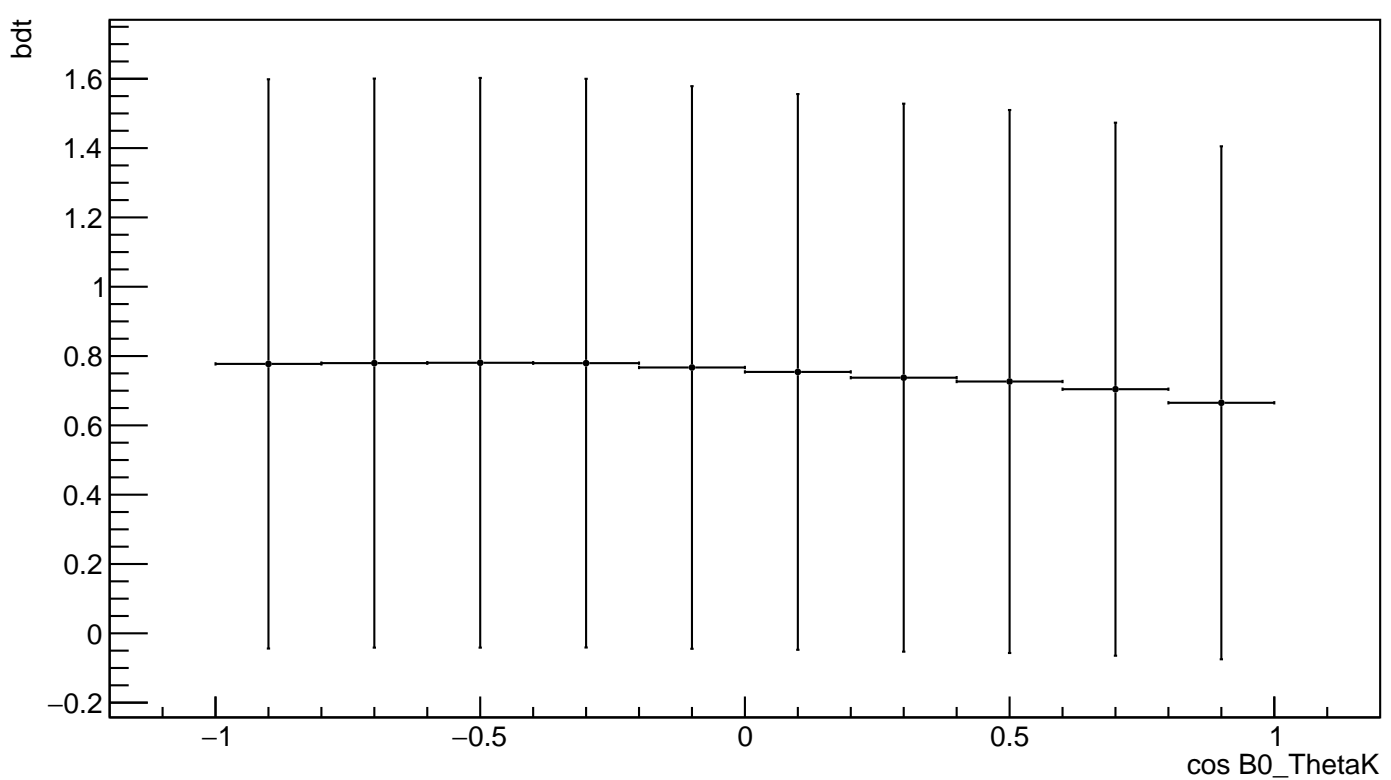
`uBoost_plot_bdt_vs_B0_ThetaL`



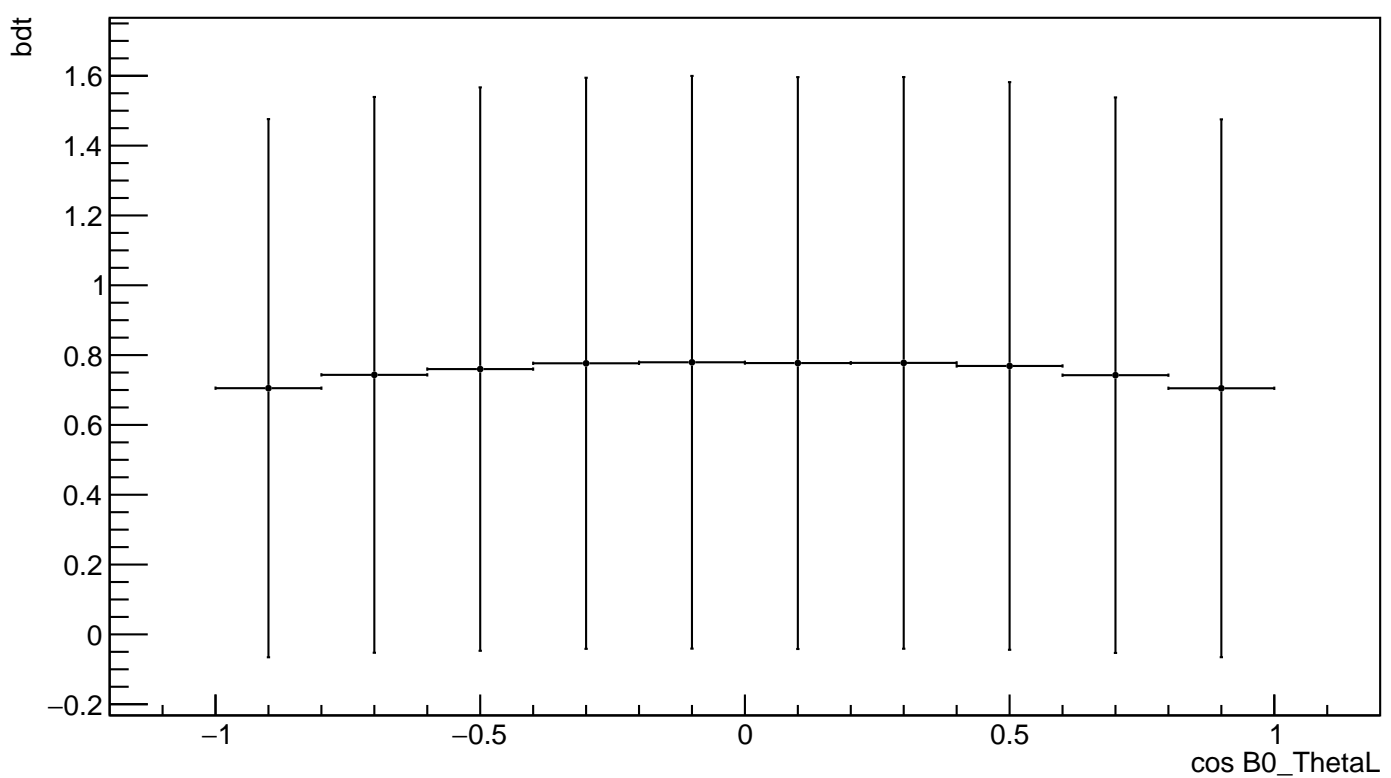
uGB+FL_plot_bdt_vs_B0_M



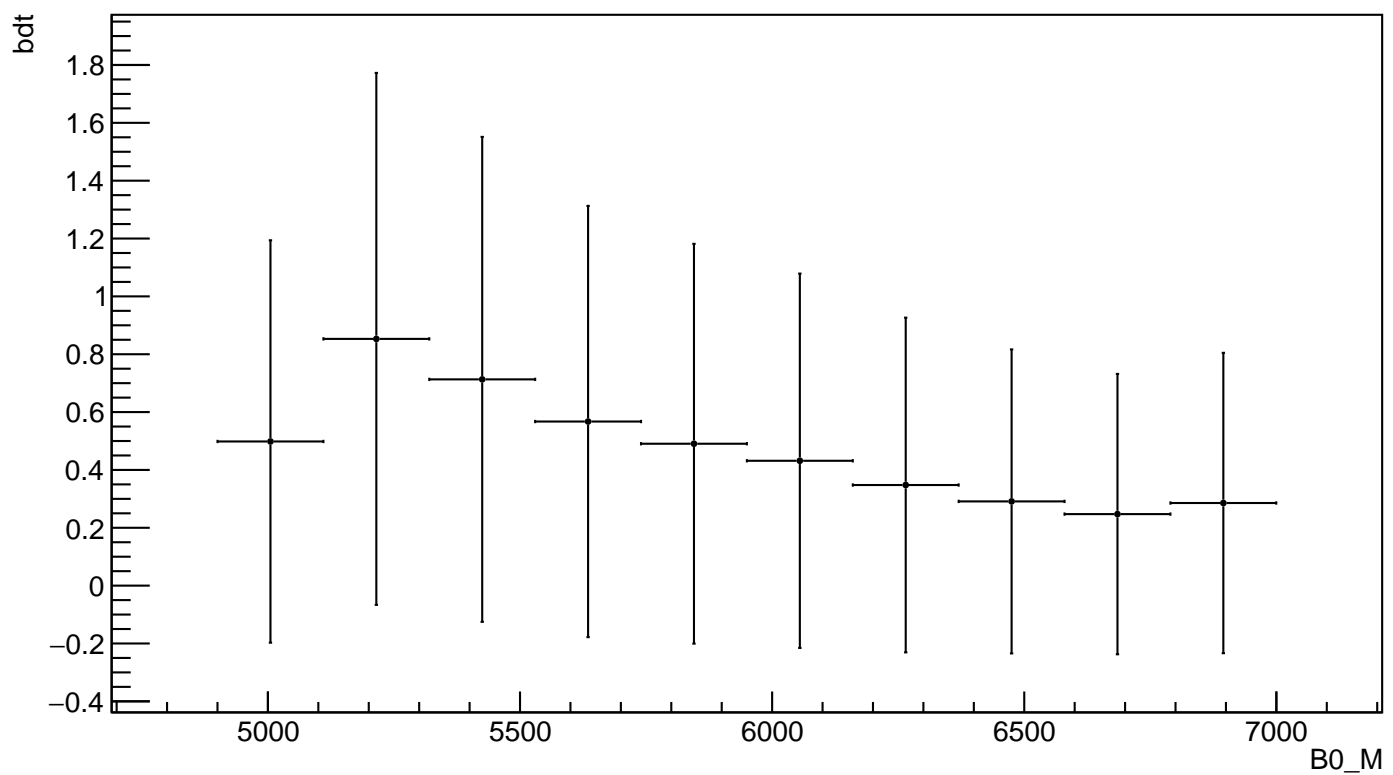
uGB+FL_plot_bdt_vs_B0_ThetaK



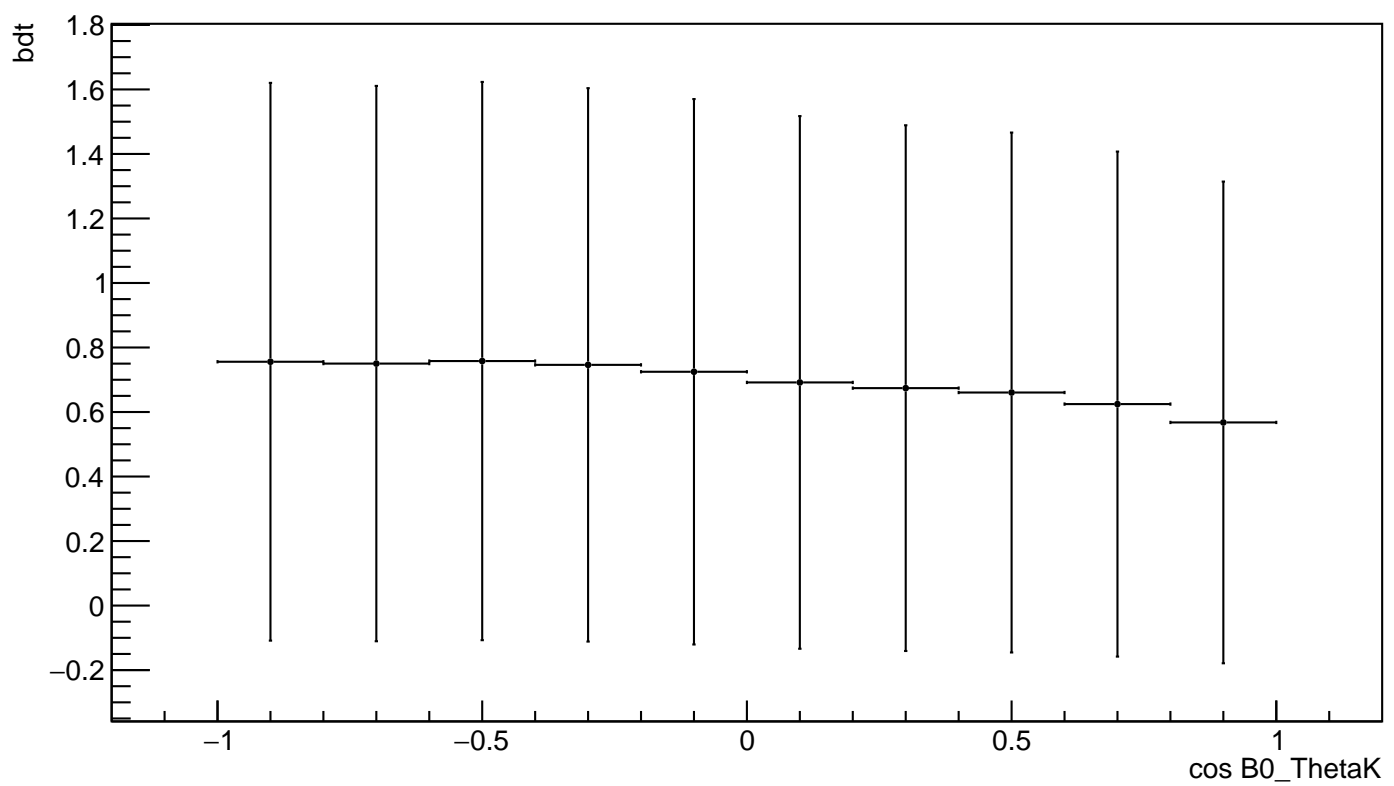
uGB+FL_plot_bdt_vs_B0_ThetaL



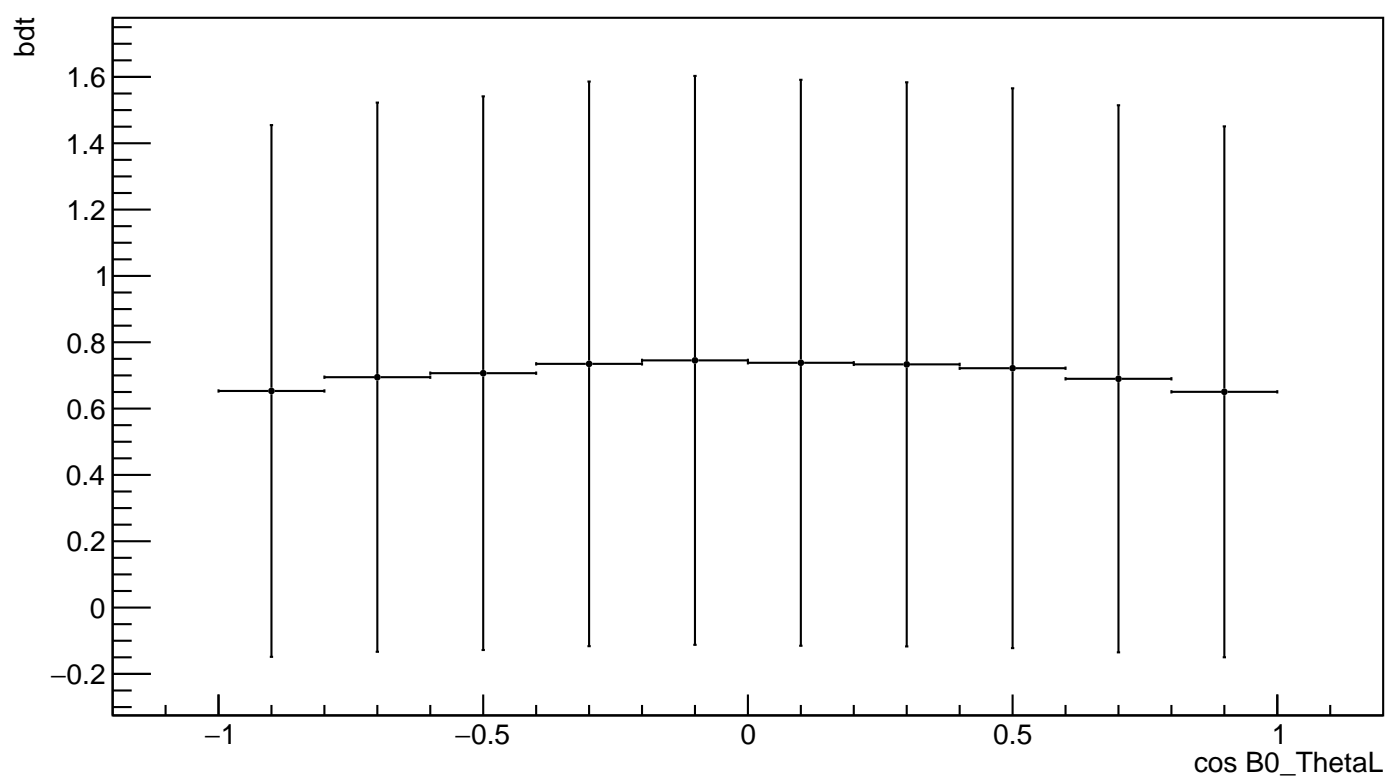
uGB+knnAda_plot_bdt_vs_B0_M



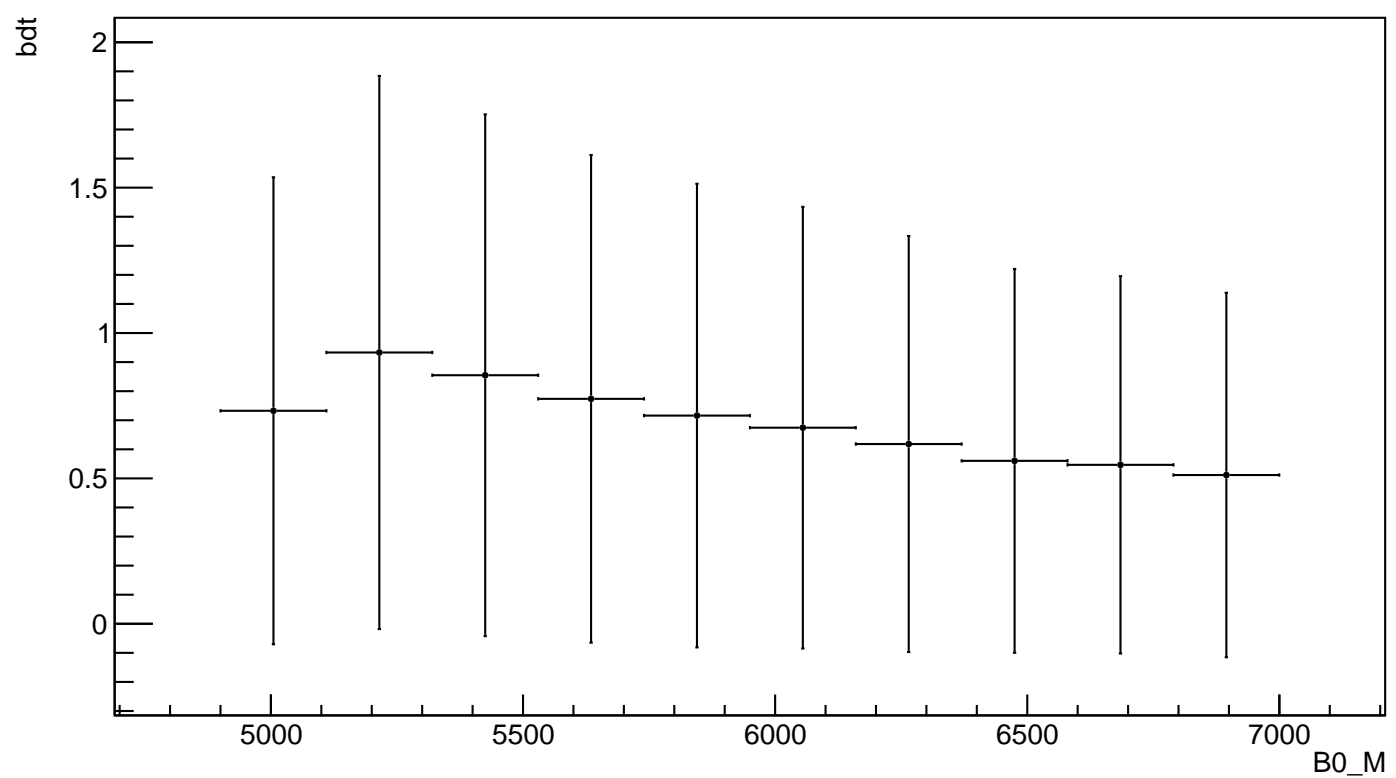
`uGB+knnAda_plot_bdt_vs_B0_ThetaK`



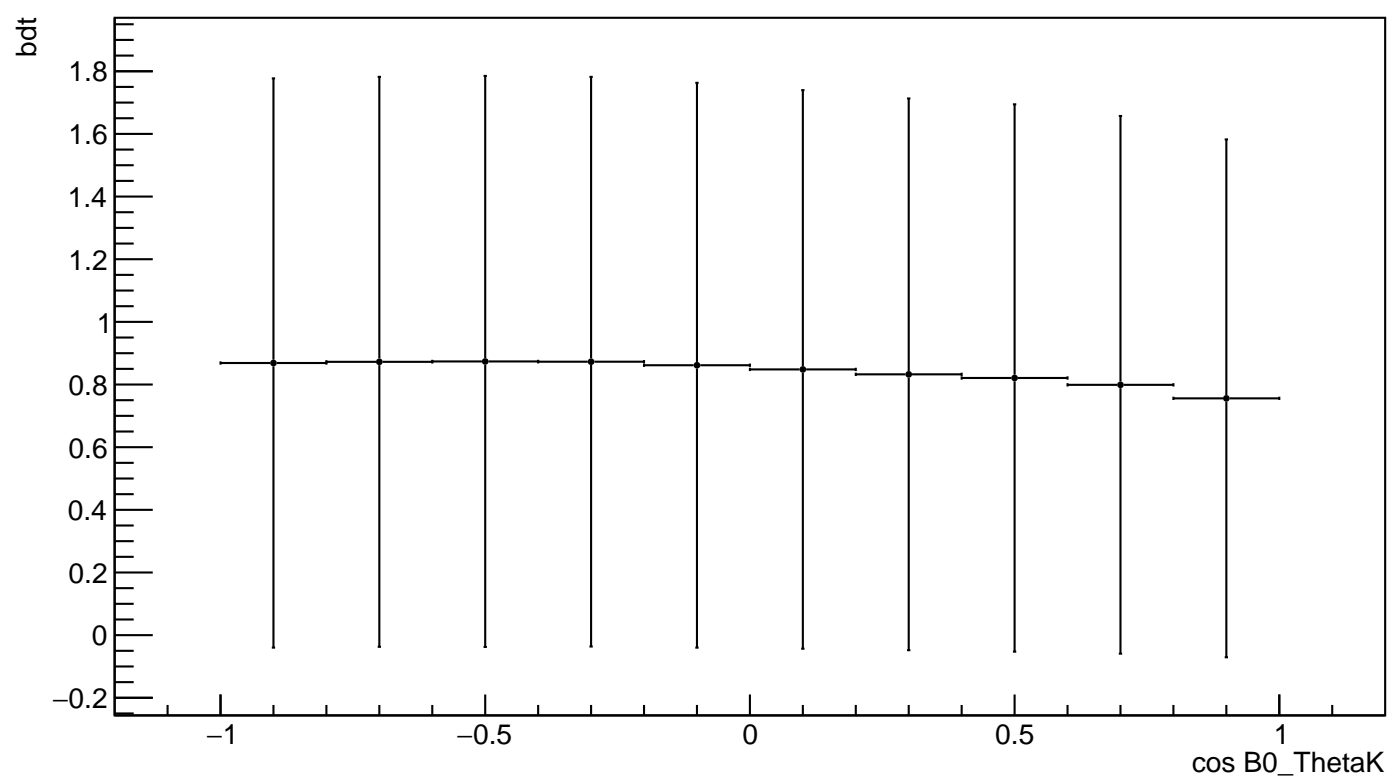
uGB+knnAda_plot_bdt_vs_B0_ThetaL



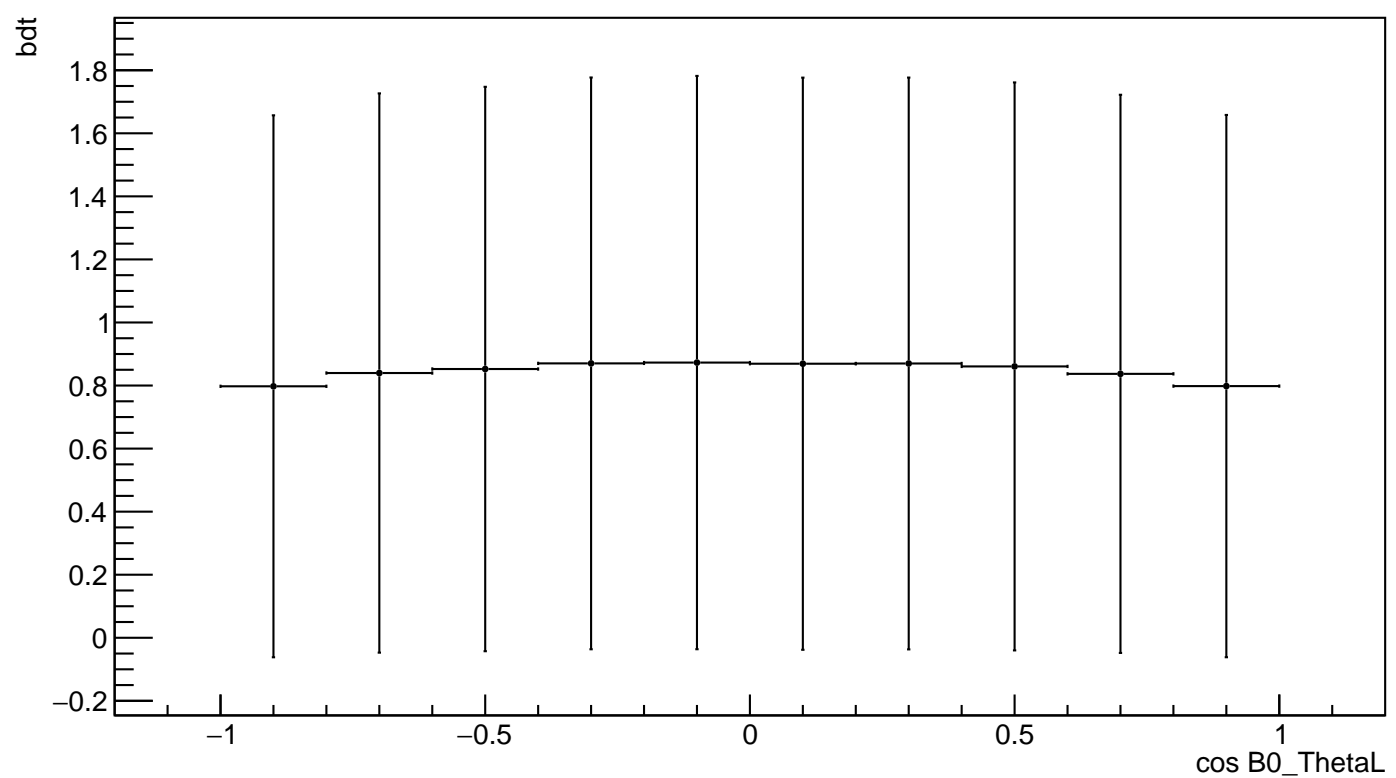
xgb_plot_bdt_vs_B0_M



xgb_plot_bdt_vs_B0_ThetaK



xgb_plot_bdt_vs_B0_ThetaL



C. Reweighting plots

